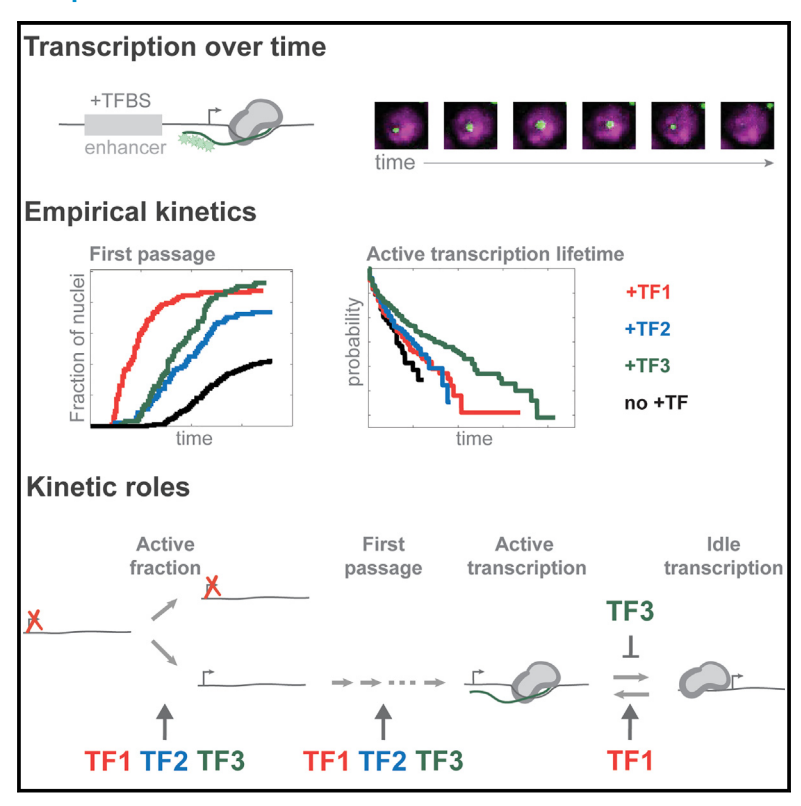
Transcriptional activators in the early *Drosophila* embryo perform different kinetic roles

Graphical abstract



Authors

Timothy T. Harden, Ben J. Vincent, Angela H. DePace

Correspondence

angela_depace@hms.harvard.edu

In brief

We demonstrate that in animals, the proteins that control gene expression can activate a gene in different ways. Our results support a mechanism called kinetic synergy, where proteins with distinct dynamic roles collaborate to turn on a gene.

Highlights

- TFs can perform distinguishable kinetic roles when activating the transcription
- Individual TFs can perform multiple kinetic roles, some of which overlap with other TFs
- We use a simple method to infer kinetic roles using live imaging
- We used coarse-grained, empirical math models to compare kinetic roles









Article

Transcriptional activators in the early *Drosophila* embryo perform different kinetic roles

Timothy T. Harden, 1 Ben J. Vincent, 1,2 and Angela H. DePace1,3,*

- ¹Department of Systems Biology, Harvard Medical School, Boston, MA 02115, USA
- ²Present address: Department of Biological Sciences, University of Pittsburgh, Pittsburgh, PA 15260, USA
- *Correspondence: angela_depace@hms.harvard.edu https://doi.org/10.1016/j.cels.2023.03.006

SUMMARY

Combinatorial regulation of gene expression by transcription factors (TFs) may in part arise from kinetic synergy—wherein TFs regulate different steps in the transcription cycle. Kinetic synergy requires that TFs play distinguishable kinetic roles. Here, we used live imaging to determine the kinetic roles of three TFs that activate transcription in the *Drosophila* embryo—Zelda, Bicoid, and Stat92E—by introducing their binding sites into the *even-skipped* stripe 2 enhancer. These TFs influence different sets of kinetic parameters, and their influence can change over time. All three TFs increased the fraction of transcriptionally active nuclei; Zelda also shortened the first-passage time into transcription and regulated the interval between transcription events. Stat92E also increased the lifetimes of active transcription. Different TFs can therefore play distinct kinetic roles in activating the transcription. This has consequences for understanding the composition and flexibility of regulatory DNA sequences and the biochemical function of TFs. A record of this paper's transparent peer review process is included in the supplemental information.

INTRODUCTION

In all cells, gene transcription is activated or repressed by a collection of transcription factor proteins (TFs) that bind their cognate DNA target sequence and, together, regulate transcription. TFs can interact either directly with one another or indirectly, through cofactor proteins, to synergistically regulate the transcription. Alternatively, synergistic expressions may arise from the regulation of different rate-limiting steps in the kinetic pathway of transcriptions. Kinetic synergy requires that different TFs regulate distinct kinetic steps and thus have distinguishable kinetic roles. Here, to test the feasibility of kinetic synergy, we characterize the kinetic roles of three TFs active during Drosophila melanogaster development, using live imaging and mathematical modeling.

Some TFs downregulate transcription—repressors—whereas other TFs upregulate transcription—activators. ^{4,5} These labels assign individual proteins to a broad class of functional activities. Since the advent of this activator/repressor paradigm, ⁶ functional subclasses of activators and repressors have been delineated by assigning more specific mechanistic labels to individual TFs. For example, pioneer factors open local chromatin allowing subsequent binding of other factors⁷; short- and long-range repressors work to silence nearby or distally bound activators, respectively^{8,9}; and bifunctional factors exhibit context-dependent activity with the capacity to either activate or repress transcription (e.g., Stampfelet al., ¹ Majello et al., ¹⁰ and Papatsenko and Levine¹¹).

Aside from a handful of exceptions (e.g., Duarte et al 12), most animal TFs remain categorized as activators, repressors, or bifunctional factors. This stands in contrast to bacteria, where the activator/repressor paradigm is rich with detailed descriptions of TF mechanisms. There, biochemical and structural approaches have elucidated detailed kinetic and physical mechanisms for many individual TFs (e.g., the sigma factors 15–18). Within animal transcription, research has largely focused on a tissue-specific paradigm of TF function that identifies TFs responsible for developmental patterning and cell type specification and characterizes them as activators or repressors. 13,19,20 The stage is thus set for the animal activator/repressor paradigm to be fleshed out in greater detail, including what, if any, differences exist in the kinetic roles of TFs labeled as activators.

Mechanistic information on TF function has typically been obtained using biochemistry and fluorescence imaging. The *in vitro* reconstitution approaches that have proven indispensable in the study of bacterial transcription regulation are transferable to eukaryotic model organisms, ^{22,23} yet remain challenging. ²⁴ *In vivo* detection of nascent transcript synthesis via the MS2/MS2 coat protein (MCP) system has emerged as the technique of choice for studying transcription regulation at the level of individual genes in eukaryotes and specifically in *Drosophila melanogaster* embryos. ^{25–28} This system has been used to measure activation by individual TF proteins in the fly embryo by either quantifying changes in the TF concentration ^{29,30} or through mutation of regulatory DNA to introduce or disrupt TF binding sites. ^{31–33}



Article



For MS2/MCP experiments, the most challenging part of the technique is no longer making the measurements but rather analyzing the resulting data and deriving mechanistic conclusions from it. Many studies have measured transcription in the embryo using the MS2/MCP system (reviewed in Fernandez and Lagha³⁴ and Wissink et al.³⁵). The analytical approaches employed by these studies range from statistical quantification (e.g., Yamada et al.³² and Fukaya et al.³⁶) to various mathematical models. 30,31,33,37-40 However, the MS2/MCP measurements themselves are many biochemical steps removed from the molecular kinetics of interest, namely transcription initiation. This makes the application of predictive models derived from kinetic pathways difficult. A recent approach used a sophisticated model that identified the likely transcriptional state of the promoter over the time course of a nuclear division cycle (NC).⁴⁰ This required assuming a model of the kinetic states, in this case "on" and "off," and their transitions, then developing a hidden Markov model that infers the promoter state from the fluctuations in MS2/MCP fluorescence emissions.

Assuming a model a priori, however, is not necessary if the goal is to identify the kinetic role of TFs. Although they fall short of directly reporting the molecular state of the promoter, MS2/ MCP measurements give a highly detailed record of transcription. The kinetic role of a TF is reflected in how these records change in response to changing TF activity. Simple empirical models can be used to describe distributions derived from these records. By comparing these distributions, we can quantitatively compare TF activity and directly test a requirement of kinetic synergy that different TFs can play distinguishable kinetic roles during transcription.

The empirical models we use here to define the kinetic roles of TFs have been used previously to explicitly elucidate kinetic pathways from single-molecule in vitro transcription experiments (e.g., Friedman and Gelles¹⁵). These models assume nothing about the underlying kinetic pathway of the system. Here, because of the nature of MS2/MCP measurements, this approach cannot elucidate the kinetics of the biochemical steps that lead to transcription nor can it predict transcriptional outputs a priori. Instead, it gives insight into the function of TFs by tracking changes in model parameters—the timing and duration of MS2/MCP signal - due to increased TF activity. Ultimately, the utility of our model is not to interpolate the biochemical steps that TFs regulate, as it is incapable of that, but to compare the activity of TFs so as to establish if different activators have the same or different kinetic roles.

We characterized the kinetic roles of three activating TFs present in the early D. melanogaster embryo. Zelda (Zld) is uniformly distributed across the early embryo41 and is thought to be a pioneer factor that can establish and/or maintain open chromatin (Harrison and Eisen⁴² and references therein). Zld has been previously shown to decrease the time of first passage into transcription within the blastoderm. 30,33 Bicoid (Bcd) is a Hox3derived protein that is well known for its role in patterning the anterior-posterior axis of the embryo through a concentration gradient 43,44 and is dependent on the inter-protein cooperative interactions to activate transcription. 45-48 Stat92E (Dstat) is the signal transducer and activator of transcription (STAT) component in the Drosophila JAK/STAT pathway. 49 Dstat is uniformly distributed across the early embryo, is an essential zygotic activator, 50,51 and has been proposed to act downstream of nucleosome displacement to activate transcription.54

To decipher the kinetic roles of Zld, Bcd, and Dstat, we created transcription reporters driven by the even-skipped stripe 2 minimal enhancer (eve2) and its cognate promoter.⁵³ Activation through eve2 has been highly studied, both in terms of the cis-regulatory sequences required⁵³⁻⁵⁶ and the spatiotemporal pattern it drives. 57-59 This makes eve2 an ideal substrate for this detailed kinetic study.

Here, we used MS2/MCP transcription reporters and empirical modeling to compare and contrast the kinetic roles of three activating TFs. Transcriptional dynamics driven by variants of eve2 containing additional binding motif sequences for Zld, Bcd, and Dsat were compared with the dynamics of a benchmark sequence that drives low levels of expression. We then applied a collection of chemical kinetics-based models to characterize the dynamic transcription signals driven by these sequence variants. We found that Zld, Bcd, and Dstat acted on overlapping but unique subsets of parameters over the course of the NC 14. The kinetic role of each TF also changed over the NC. This work therefore supports the hypothesis that kinetic synergy can contribute to combinatorial control of transcription in the early fruit fly embryo.

RESULTS

eve2 separated from the promoter drives weak expression

Dynamic expression driven by eve2 has been previously measured in two contexts: the endogenous even-skipped locus^{57,58} and a transcription reporter containing the 1.7 kilobases (kb) upstream of even-skipped, which harbors eve2.59 There was a slight anterior shift in the position of stripe 2 expression over the course of NC 14 when measured in the endogenous context that was not observed in the reporter. To measure expression driven by isolated eve2 (rather than its flanking sequences, which are present in both the endogenous context and extended reporter described above), we constructed a reporter, eve2:neutral, containing eve2 and the even-skipped promoter separated by a 765 bp neutral sequence spacer (Figure 1A). The spacer sequence was computationally designed to lack predicted binding sites for TFs present in the early embryo⁶⁰ (see STAR Methods). The spacer length is comparable, although not identical, with the distance between eve2 and the eve promoter at the endogenous locus (1,033 bp). We did not place the enhancer immediately upstream of the promoter because TFs bound to enhancers immediately adjacent to the promoter can act differently than they do when placed at a distance. 61,62 The reporter contained 24 tandem repeats of an MS2 binding motif sequence (MBS)⁶³ in the 5' untranslated region of a transcription unit (see STAR Methods) and was integrated into the attP2 landing pad site using phiC31-mediated transgenesis.⁶⁴

Living embryos were imaged by dual-inverted selective plane illumination microscopy (diSPIM).65 Previous studies have used confocal microscopy, 33,36,61,66-68 which relies on oil-immersion objective lenses and requires subjecting the embryos to continuous submersion in halocarbon oil before and during imaging. By contrast, diSPIM relies on water-immersion objective lenses, allowing dechorionated embryos to be placed on a single coverslip



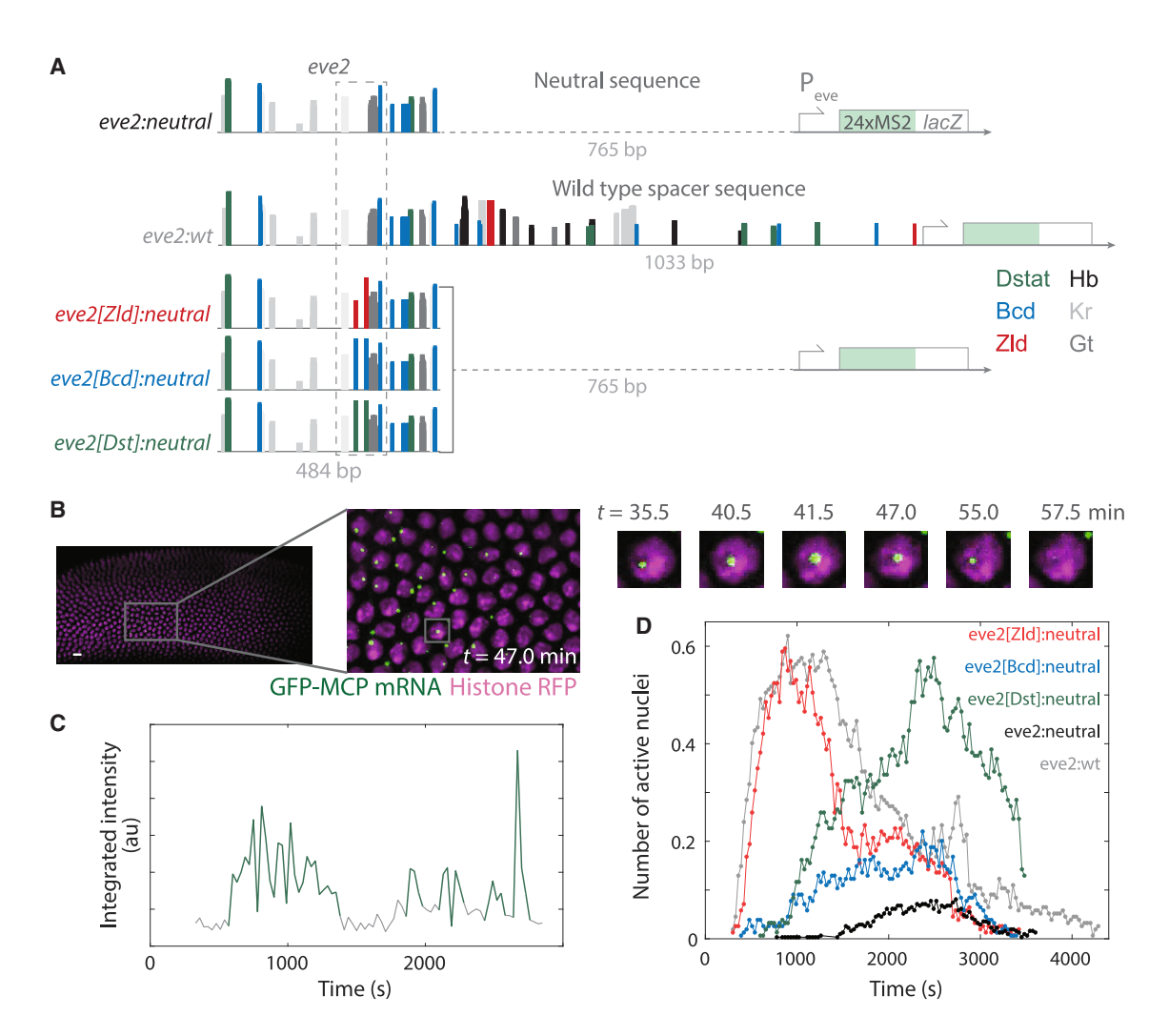


Figure 1. Measuring the activity of individual TFs against benchmark regulatory sequences

(A) Schematics of the minimal even-skipped stripe two enhancer (eve2) transcription reporter constructs. Each contains the even-skipped promoter driving expression of 24 repeats of the MS2 stem-loop sequence followed by a partial sequence of the bacterial lacZ operon. eve2:neutral contains a spacer sequence with no predicted transcription factor binding sites (dashed line). eve2:wt is eve2 with a spacer containing the wild-type locus sequence between the enhancer and the promoter. The three transcription factor reporters - eve2[ZId]:neutral, eve2[Bcd]:neutral, and eve2[Dst]:neutral - are identical to eve2:neutral but contain two mutations to add predicted binding motifs for a single transcription activator (dashed box), either Zld, Bcd, or Dstat, respectively. Colored bars are transscription factor binding sites predicted by the software SiteOut. 60 Hb, Kr, and Gt stand for Hunchback, Kruppel, and Giant, respectively.

(B) Left: image of a 2D maximum projection of the diSPIM microscope field of view with histone-red fluorescent protein (magenta) and GFP-MS2 coat protein (green). Gallery images: magnified view of the marked region over time showing a detected active transcription locus. t = 0 corresponds to the beginning of nuclear cycle 14. Scale bars, 10 μm.

(C) Example MCP-GFP fluorescence emission record from a single nucleus during NC 14. Green marks detected active transcription signal; gray marks intervals during which no fluorescent signal was detected.

(D) Dynamic transcription profiles during NC 14 for the constructs in (A). Binary detection of the number of detected active transcription loci within the microscope field of view from two replicate experiments for each construct. There are 4,535 loci detected across 114 active nuclei for eve2:neutral, 5,265 loci from 238 nuclei for eve2:wt, 3,631 loci from 289 nuclei for eve2[Zld]:neutral, 1,512 loci from 113 nuclei for eve2[Bcd]:neutral, and 4,535 loci from 207 nuclei for eve2[Dst]:neutral.

and imaged while in a bath of Schneider's media (STAR Methods). We found that embryos were equally viable when imaged using both techniques. 61 However, diSPIM has other advantages, namely decreased photobleaching rates and phototoxicity for a comparable signal-to-noise ratio, ^{69–71} without the loss of spatial or temporal resolution. Here, we chose an excitation laser power and image acquisition frequency that did not artificially shorten MCP-green fluorescent protein (GFP) signal dwell times through photobleaching and minimized any

bias toward long dwell times (i.e., did not miss short dwell times; see Figure S1 and STAR Methods).

We observed the appearance of the MCP-GFP signal as diffraction-limited spots above the background (Figure 1B). This signal was colocalized with the histone-red fluorescent protein (his-RFP) signal, reflecting the binding of many MCP-GFP proteins to nascent RNA in complex with actively transcribing RNA polymerase II proteins (RNA Pol II) within individual nucleus.⁷² As in previous studies, we interpreted the appearance

Article



of signal from the MBS repeats as the start of active transcription. ^{67,68,73} When the transcription signal later disappeared, presumably due to transcript termination by most or all actively transcribing RNA Pol II and subsequent release of the fluorescently tagged mRNA, this was scored as the end of active transcription.

Scoring genuine active transcription from MS2/MCP records is challenging due to inherent extrinsic noise. We therefore determine instances of active transcription using integrated fluorescence intensity, size, and shape of MS2/MCP signal and hysteresis. To account for size and shape, we assume that actual transcription gives rise to a signal that is well described by a two-dimensional Gaussian. We also assume that single frame dropouts (where fluorescence decreases abruptly) are an experimental artifact; we therefore allow for hysteresis in tracking spots to avoid scoring artificially short records. We report binary transcription signals; thus, none of the measurements reported here rely on fluctuations in signal intensity. We chose this approach in an attempt to minimize biases that may arise from artifacts that contribute to large fluctuations in MS2/MCP signal intensity. Representative fluorescence intensity records, along with a detailed description of how transcription was scored, are in Figure S2.

For each imaging replicate, acquisition began during NC 13, and analysis was performed on all time points from the start of NC 14, defined here as the end of anaphase, until the onset of gastrulation. In a comparison of biological replicates, we found the distributions derived from the MCP-GFP transcript signal were largely indistinguishable, save for those of eve2:neutral, which drove weaker expression (Figure S4). For eve2:neutral, no nuclei exhibited MCP-GFP signal above detection threshold until ~20 min into NC 14 (Figure 1D, black curve), compared with <10 min reported by Bothma et al. for an MS2 reporter driven by eve2 flanked by sequences from the endogenous even-skipped locus. In addition, transcription driven by eve2:neutral was detected in a small number of nuclei compared with that same reporter.⁵⁹ We thus acquired additional replicates of eve2:neutral. All data wrangling and analysis were conducted with custom MATLAB software that was in part adapted from an existing platform (see data and code availability).7

Active transcription was not observed outside the stripe 2 pattern during NC 14, except in select cases, wherein the transcript signal was detected within the domain of eve stripe 7, which was expected, given previous reports that used transcription reporters for eve2. ^{59,75–77} The anterior and posterior edges of the stripe 2 domain are set by repressor proteins, including Giant and Kruppel, that bind to sequences within eve2. ^{53,78} We limited our analysis to the nuclei located in the center of the stripe (Figure S3), where these repressive interactions are minimized, in an attempt to isolate activating TF activity from repressive TF activity. Oftentimes, we observed multiple instances of active transcription within the same nucleus (e.g., Figure 1C, green), consistent with a previous study of eve2. ⁵⁹

An extended region upstream of even-skipped that includes eve2 drives a normal pattern of expression

To investigate the cause of the weak expression driven by eve2:neutral, we created a second reporter, eve2:wt, containing a 1,517 bp sequence identical to the 5' region of the endogenous

even-skipped locus, composed of eve2 and the 1,033 bp sequence between eve2 and the promoter (Figure 1A). The 1,033 bp endogenous sequence contains multiple predicted TF binding motifs, including those for Bcd, Zld, and DStat. eve2:wt was also integrated into attP2 and imaged as described above.

In contrast to *eve2:neutral*, *eve2:wt* drove early, persistent transcription (Figure 1D, gray curve) in nearly all the nuclei within the center of the stripe 2 domain (Figure S1). Transcription driven by *eve2:wt* was detected earlier in the NC, occurred in more nuclei, and was more persistent throughout NC 14. This is consistent with a previous study where an MS2 reporter driven by a similar extended version of *eve2* was shown to drive a normal pattern of expression. ⁵⁹

Designing regulatory sequences to measure the activity of individual TFs

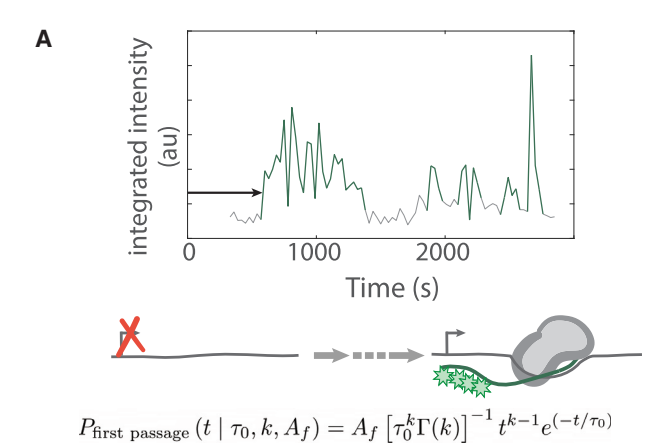
Our strategy to measure the kinetic roles of different activating TFs was to add binding sites for those TFs to an enhancer scaffold and measure the resulting differences in expressions. This required a scaffold where the consequences of additional activation are not obscured by a high baseline of the transcription signal. In previous studies, high levels of activity were thought to obscure the detection of transcriptional bursts. 36,67,68 The eve2:neutral reporter, with its weak basal expression, provides this scaffold. We therefore created a set of variants of eve2:neutral designed to recruit additional specific TFs to the reporter. For each variant, we introduced two DNA binding motifs for a single TF-either Zld, Bcd, or Dstat-by making two short-sequence mutations (8-10 nucleotides) in the same location in eve2, chosen to minimize the disruption to other TF binding sites (see STAR Methods). Each of these activating TF reporters-eve2 [Zld]:neutral, eve2[Bcd]:neutral, and eve2[Dst]:neutral-were incorporated into attP2 and imaged as above (Figure 1A). Note that eve2:wt acts as an approximation of the upper-bound for transcription activation by eve2:neutral and its variants and is therefore an informative benchmark for qualitative comparisons. However, all quantitative comparisons that follow are between eve2:neutral and its variants, the TF reporters.

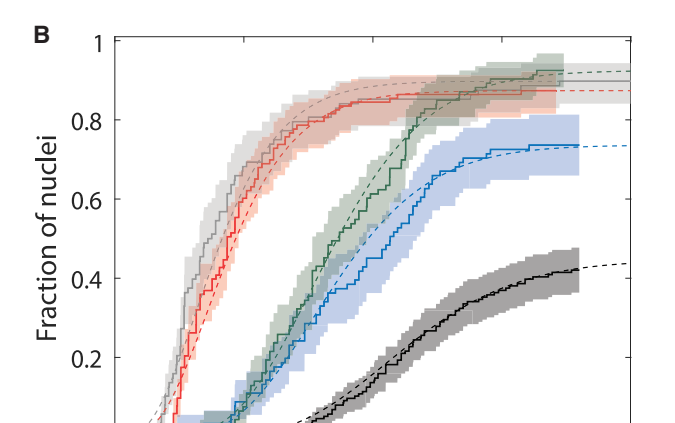
All three of the TF reporters induced transcription that exceeded that of eve2:neutral. Each dramatically altered the dynamic transcription profile (Figure 1D) and did so in a unique way. eve2[Bcd]:neutral-induced transcription similar to that of eve2:neutral but earlier and in a greater number of nuclei. eve2 [Dst]:neutral and eve2[Zld]:neutral also induced transcription earlier than eve2:neutral but in far more nuclei, similar to that of eve2:wt. However, the timing of activation by eve2[Dst]:neutral and eve2[Zld]:neutral was different. The dynamic transcription profile of eve2[Zld]:neutral peaked early in the NC then decayed quickly, again similar to eve2:wt, whereas that of eve2[Dst]:neutral had a later, broader peak. To make quantitative comparisons between the TF reporters, we employed a collection of simple empirical models, as described in the next section.

Empirical kinetic models distinguish the roles of Zld, Bcd, and Dstat in regulating transcription

We analyzed the transcription records for eve2:neutral and each TF reporter and report the distributions of three different measurements—the first-passage time, the active transcription







0 1000 2000 3000 4000 Time (s) eve2:neutral eve2[Zld]:neutral eve2[Dst]:neutral eve2:wt eve2[Bcd]:neutral

Figure 2. First-passage activation kinetics

0

(A) Graphical depiction of a first passage into transcription measurement. Emission record as in Figure 1C. The arrow denotes the first-passage time for this nucleus. Cartoon: during this interval the transcription reporter transitions from a state incapable of activating transcription (left), through a number of rate-limiting steps (dashed arrow), to a transcriptionally competent one that activates transcription (right). The mathematical model (Equation 1) is shown at the bottom.

(B) Cumulative first-passage distributions (solid curves) overlaid with a model (Equation 1, dashed curves) with the characteristic number of rate-limiting steps, k, a characteristic time constant for each of those steps, τ_0 , and the fraction of active nuclei within the center of the stripe, A_r ; see Table 1 for parameter values. The curves are normalized to the total number of nuclei in the center of the stripe (see Figure S3). There were 74 active nuclei and 166 nuclei total in the center of the stripe for eve2:neutral; 79/88 nuclei were active in the center of the strip for eve2:neutral; 79/80 nuclei were active in the center of the strip for eve2:neutral. Shaded regions represent the 90% confidence intervals from bootstrapping methods (see STAR Methods).

lifetime, and the idle period—which we explain below. These MS2/MCP measurements are straightforward and their distributions are simple to extract from any live imaging dataset (see discussion). To analyze the shape of these distributions and to compare across constructs, we used models commonly em-

ployed in the analysis of single-molecule data. These models produce characteristic distributions, and we asked how well they fit our data. The Multiple models were compared with each experimental distribution, and the adequate fit was assessed by how well the features of the experimental distribution were reproduced by the model. Adequate fits yield a set of parameters that we compare between constructs to assess the ways in which the kinetic roles of these TFs are similar or different. However, we emphasize that the absolute values of these parameters are not necessarily informative, but their values relative to one another are. Because the number and affinity of binding sites for each of Zld, Bcd, and Dstat differ within eve2, we made direct comparisons between each TF reporter and eve2:neutral.

First-passage times

There are dramatic differences in the dynamic transcription profiles of the TF reporters at early time points (Figure 1D). These differences are represented in the distributions of first-passage times when transcription is first detected in each nucleus in NC 14 (Figure 2). These distributions have three important features related to the mechanisms that lead to the first passage into transcription. First, the maximum slope of the distribution is related to the rate of initial transcription activation across the stripe pattern. Second, the plateau of the distribution is the fraction of active nuclei within the stripe. Third, the time delay between the end of anaphase (i.e., t = 0 in Figure 2B) and the first detection of transcription within the stripe 2 domain (e.g., Figure 2B t =300 s and t = 1,260 s for eve2:wt and eve2:neutral, respectively) is related to the number and length of kinetic states that regulatory DNA must pass through before reaching a state capable of initiating transcription.

Choosing a model to describe the first-passage distributions has been challenging for researchers working with MS2/MCP data. 30,33,39 One approach has been to ignore the time delay following the end of anaphase and only consider the first-passage times once transcription has been detected in any nucleus across the entire pattern (as in Dufourt et al. 33). This is reasonable since transcription cannot take place during mitosis - a process called mitotic repression.^{79,80} We initially ignored the time delay and attempted to apply the same models that are used to describe single-molecule kinetics.74 These models performed poorly. However, they taught us that the observed first-passage distributions cannot be explained by a kinetic pathway with less than 3 transcriptionally silent, rate-limiting steps (explained in Figure S5). In addition, note that the time delay varies by \sim 900 s between the five different reporters (Figure 2B). This is difficult to reconcile with the general mechanism of mitotic repression, which would act similarly across reporters. These data suggest that TFs are acting to shorten this time delay (see discussion). We therefore employed a model that can accommodate both of these observations. Namely, more than two transcriptionally silent slow steps and highly variable time delays following mitosis.

A critical choice for implementing this type of model concerns the characteristic time constants associated with each transcriptionally silent step. Although it is unlikely that they are all equivalent, it is reasonable to assume that they are each of the same order of magnitude. ^{2,23} We chose to assume the time constant of each silent step is equal. This decision was made for a couple of reasons. First, it kept the number of free parameters

Article



Table 1. First passage into active transcription model parameters

	A_f	k	$ au_0$
eve2:neutral	0.45 ± 0.04	11.3 ± 1.2	205 ± 20 s
eve2:wt	0.90 ± 0.03	4.1 ± 0.4	
eve2[Zld]:neutral	0.87 ± 0.04	4.4 ± 0.5	
eve2[Bcd]:neutral	0.74 ± 0.05	8.5 ± 1.0	
eve2[Dst]:neutral	0.92 ± 0.06	8.5 ± 0.9	

See Equation 1. The characteristic lifetime for all rate-limiting steps, τ_0 , was globally fit to all five transgenic reporters. Standard errors were computed using bootstrapping methods (see STAR Methods).

lower than a model that allowed the rate of each silent step to vary independently. Second, we had little *a priori* evidence of what, biologically, these silent steps might represent and what their cognate rates might be. Finally, this choice aligns with previous studies. ^{30,33} From this, we are forced to assume that the number of rate-limiting steps must change to account for the differences in the first-passage distributions in Figure 2B. This is not to say that the kinetic pathway itself changes, only that under different circumstances, some steps become fast and are no longer rate limiting. Finally, due to the limitations of the perturbations here, the model must be agnostic to exactly what the rate-limiting steps represent biochemically and the order in which they occur. We discuss other modeling options in the discussion.

From these choices, we arrived at a linear kinetic model of several steps, each with an equivalent characteristic time constant. Each step is assumed to be irreversible. This simplifying assumption is likely not appropriate for every step in the kinetic pathway, but mathematically, the mean rate of transcription from any linear kinetic scheme containing reversible steps can be substituted by an equivalent scheme of irreversible steps through the addition of pseudo-steps that do not represent biochemical reactions.² Therefore, the qualitative conclusions here will likely be unchanged even if the true kinetic scheme contains reversible steps. We emphasize that our question is simply whether the kinetic roles of individual TFs are distinguishable; this does not require a strict interpretation of the actual values of the parameters, only their relative values.

Statistical assessments of error for this and other models were assumed to lie at the level of individual nuclei and not at the level of individual embryos. This approach is common with data from single nuclei. This assumption is reasonable, considering that within the same nucleus, transcriptions from two alleles of the same gene are not strongly correlated. In addition, we have (1) limited the analysis to a narrow region within the center of the stripe 2 pattern (Figure S3), where the extra-nuclear environment is similar, and (2) limited the measurements that we report to those which do not obviously suffer from embryo-to-embryo variability, such as pattern border location. This strategy fortuitously confers the statistical power of many independent measurements (i.e., nuclei) onto these data, rather than a few (i.e., embryos; see STAR Methods and Figure S4).

We described the first-passage distributions with a gamma distribution model (a generalization of the Poisson distribution):

$$P_{\text{first passage}}^{i}(t|\tau_{0},k^{i},A_{f}^{i}) = A_{f}^{i} \left[(\tau_{0})^{k^{i}} \Gamma(k^{i}) \right]^{-1} t^{k^{i}-1} \exp(-t/\tau_{0})$$
(Equation 1)

Where $i \equiv eve2:wt$, eve2:neutral, eve2[Zld]:neutral, eve2[Bcd]: neutral, or eve2[Dst]:neutral. A_f is the active fraction of nuclei in the center of the stripe, τ_0 and k are the gamma distribution scale and shape parameters, respectively, and Γ is the gamma function (Figure 2B, smooth curves; Table 1). Gamma distributions have been applied in various contexts of biology, for example, to determine the mechanism of molecular motors from single-molecule data. He Dufourt et al. did so for the measurements similar to those in Figure 2. Let ^{33}k can be interpreted as the average number of rate-limiting steps, whereas τ_0 can be interpreted as the characteristic time constant of each of these steps. Here, we chose to fit the time constant, τ_0 , globally to all five reporter datasets while simultaneously fitting the number of steps, k, independently for each reporter construct (see STAR Methods for an explanation of this choice).

From the model, the first-passage distributions can be explained by varying numbers of rate-limiting steps, each with a characteristic time of 205 ± 20 s. Each of the activating TF reporters increased the active fraction of nuclei within the stripe relative to eve2:neutral (A_f in Table 1). This quantifies what would be expected from inspection of the dynamic transcription profiles in Figure 1D. In addition, all reporters decreased the number of rate-limiting steps relative to eve2: neutral: $k = 11.3 \pm 1.2$ for eve2:neutral, 8.5 ± 1.0 and $8.5 \pm$ 0.9 for eve2[Bcd]:neutral and eve2[Dst]:neutral, respectively, and 4.1 \pm 0.4 and 4.4 \pm 0.5 for eve2:wt and eve2[ZId]: neutral, respectively. Regardless of the detailed interpretation of this model, it is clear that although all reporters reduce the number of rate-limiting steps on the path to first-passage transcription activation, those that bind Zld (eve2:wt and eve2 [Zld]:neutral) do so to a large extent. This explains much of the differences in the dynamic transcription profiles of Figure 1D, but not entirely. The TF reporters must be acting to tune other kinetic parameters in addition to the first-passage time.

Active transcription lifetimes

An active transcription lifetime is the time over which a signal is continuously detected within a single nucleus (Figure 3A). This value is proportional to the number of RNA molecules synthesized during that time interval.⁵⁹ The cumulative distributions in Figure 3B show the survival of the active transcription lifetimes. The rate at which these curves fall off for increasing active transcription dwell time (i.e., the slope) is proportional to the rate by which active transcription turns off (see STAR Methods).

These curves can reveal one or more types of activation present in the distribution, each type defined by a characteristic lifetime. The for example, the distributions in Figure 3B do not reflect the presence of a single characteristic lifetime (Figure S6). They are not straight but kinked; the kink separates two regions of the curves, each with a distinct slope. This led us to apply a biexponential probability density function, which is commonly used to describe chemical kinetics (e.g., Friedman and Gelles 15) to model these distributions:



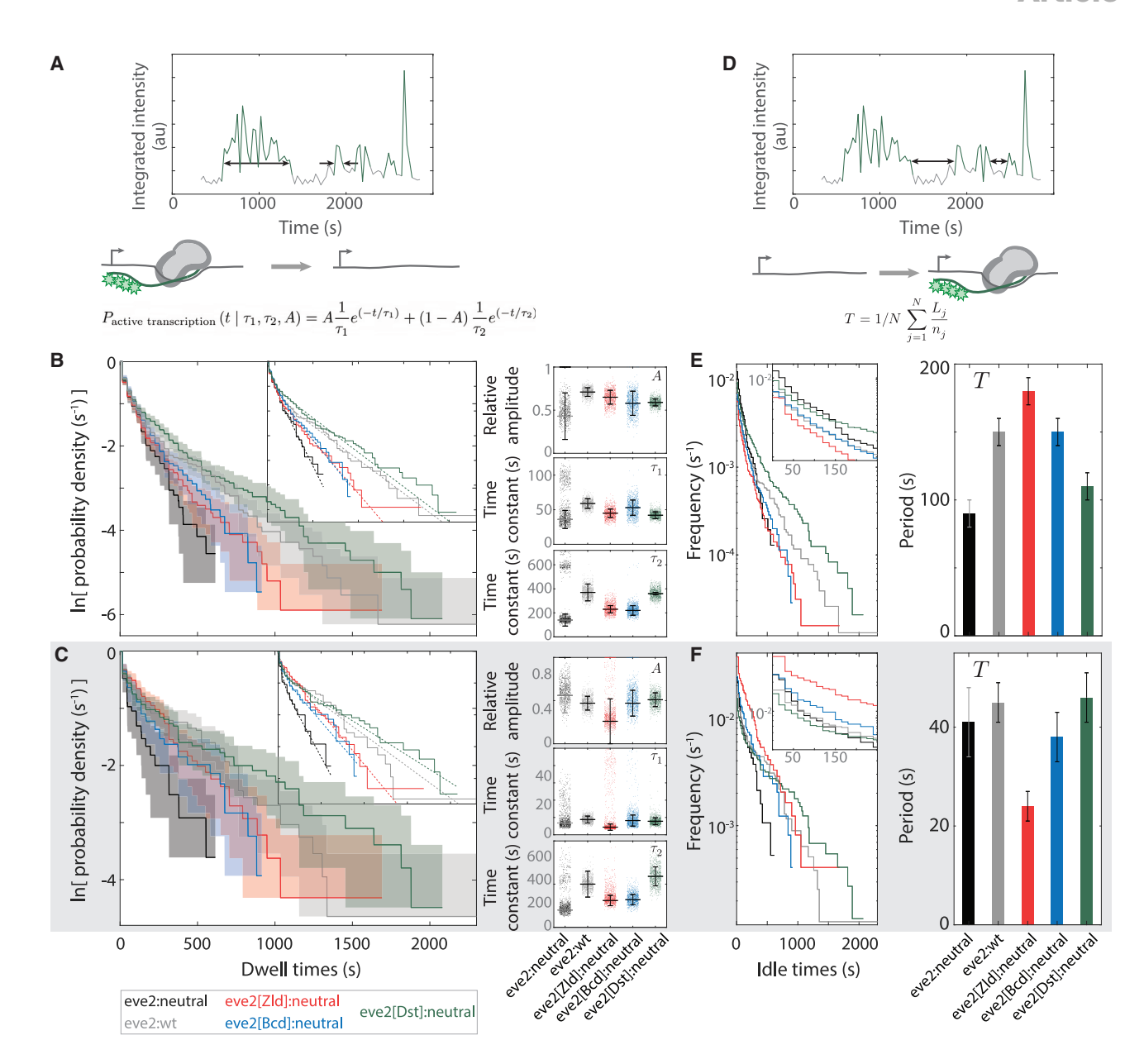


Figure 3. Active transcription and idle period kinetics

(A) Graphical depiction of active transcription lifetime measurements. The double-headed arrows denote two example intervals of active transcription. Cartoon: during these intervals, the reporter locus transitions from a state containing many RNA polymerase molecules (gray bean) undergoing RNA synthesis (green line) to one lacking detectable active transcription (green stars). The model (Equation 2) is shown at the bottom.

(B) Cumulative lifetime distributions of active transcription (solid curves). n = 190, 507, 363, 236, and 444 for eve2:neutral, eve2:wt, eve2[ZId]:neutral, eve2 [Bcd]:neutral, and eve2[Dst]:neutral, respectively. Data are overlaid with a model (Equation 2; dashed curves). Shaded regions represent 90% confidence intervals from bootstrapping methods using 10,000 simulated datasets (STAR Methods). The mean and standard error of the model parameters, time constants τ_1 and τ_2 , and relative amplitude A are to the right. These plots also show 1,000 randomly selected parameter sets from fitting Equation 2 to simulated data from bootstrapping (points). The bimodal nature of the eve2:neutral parameter values is due to simulated data frequently lacking a substantial long-lived population, making those distributions best characterized solely by the τ_1 parameter (with A = 1).

(C) As in (B), but the data have been partitioned into the 20% of active transcription lifetimes that first appear during NC 14 (see STAR Methods). n = 37, 104, 75, 51, and 89 for eve2:neutral, eve2[Ztd]:neutral, eve2[Bcd]:neutral, and eve2[Dst]:neutral, respectively.

(D-F) Idle transcription period. (D) Graphical depiction of idle transcription period measurements. The double-headed arrows denote two idle periods. Cartoon: during these intervals, the transcription reporter locus transitions from a state lacking active transcription to one containing many RNA polymerase molecules undergoing RNA synthesis. The model (Equation 3) is shown at the bottom. (E) Cumulative frequency distributions of the idle periods (left). The inverse of the mean idle period, in units of s⁻¹, can be read directly from these distributions via the vertical axis intercept (inset); these, along with their standard error, are depicted on the right. See Table 3. n = 116, 428, 273, 169, and 358 for eve2:neutral, eve2:wt, eve2[Zld]:neutral, eve2[Bcd]:neutral, and eve2[Dst]:neutral, respectively. (F) As in (E), but for the 20% of idle periods that first occur during NC 14.

Cell Systems **Article**



Table 2. Model parameters values for active transcription

		Α	$ au_1$	$ au_2$
All lifetimes	eve2:neutral	0.43 ± 0.12	36 ± 8 s	$140 \pm 20 \text{ s}$
	eve2:wt	0.71 ± 0.05	59 ± 7 s	$370 \pm 50 \text{ s}$
	eve2[Zld]:neutral	0.65 ± 0.09	45 ± 8 s	$230 \pm 40 \text{ s}$
	eve2[Bcd]:neutral	0.58 ± 0.12	53 ± 14 s	$220 \pm 40 \text{ s}$
	eve2[Dst]:neutral	0.59 ± 0.04	42 ± 5 s	$360 \pm 40 \text{ s}$
Early lifetimes	eve2:neutral	0.56 ± 0.12	$34 \pm 10 \text{ s}$	$200 \pm 50 \text{ s}$
	eve2:wt	0.48 ± 0.07	45 ± 10 s	$500 \pm 70 \text{ s}$
	eve2[Zld]:neutral	0.26 ± 0.16	22 ± 7 s	$310 \pm 60 \text{ s}$
	eve2[Bcd]:neutral	0.47 ± 0.12	41 ± 16 s	$320 \pm 60 \text{ s}$
	eve2[Dst]:neutral	0.51 ± 0.08	$39 \pm 9 s$	$600 \pm 120 \text{ s}$
Later lifetimes	eve2:neutral	0.38 ± 0.27	34 ± 12 s	$120 \pm 40 \text{ s}$
	eve2:wt	0.78 ± 0.10	63 ± 12 s	$280 \pm 80 \text{ s}$
	eve2[Zld]:neutral	0.68 ± 0.15	44 ± 10 s	$150 \pm 50 s$
	eve2[Bcd]:neutral	0.48 ± 0.24	$48 \pm 17 \text{ s}$	$160 \pm 50 \text{ s}$
	eve2[Dst]:neutral	0.56 ± 0.06	40 ± 5 s	$270 \pm 30 \text{ s}$

See Equation 2. Early lifetime distributions are composed of the first 20% of active transcription intervals detected for each reporter. Later distributions are composed of the other 80%. Standard errors were computed using bootstrapping methods.

$$P_{\text{active transcription}}^{i}(t|\tau_{1}^{i},\tau_{2}^{i},A^{i}) = A^{i}\frac{1}{\tau_{1}^{i}}e^{\left(-t/\tau_{1}^{i}\right)} + \left(1-A^{i}\right)\frac{1}{\tau_{2}^{i}}e^{\left(-t/\tau_{2}^{i}\right)}$$
(Equation 2)

Where τ_1 and τ_2 are characteristic lifetimes, and A and 1 – A are the relative amplitudes of each, respectively (Figure 3B, smooth curves). These parameters were determined by maximum likelihood fitting to the distributions of active transcription lifetimes (Table 2; see STAR Methods). The slope of the model over short lifetimes is proportional to the inverse of a short-lived characteristic time, τ_1 , and the slope at longer dwell times is proportional to the inverse of a second, longer-lived characteristic time, τ_2 . In other words, once activated, for both eve2:neutral and eve2:wt, transcription does not turn off stochastically with a single characteristic lifetime.

Kinetically, each of these two types of activations represents a state of the system, each of which contributes to both terms in Equation 2. The exact details of the biochemical identities, stability, and pathways of these states cannot be determined from the data and analysis here.

The model in Equation 2 revealed the kinetic differences between activation by eve2:wt and activation by eve2:neutral. The apparent increase in transcription driven by eve2:wt was due to longer characteristic times, τ_1 and τ_2 , as would be expected a priori. However, an interesting wrinkle emerged from the application of the model. The fraction of long-lived lifetimes, (1 - A), was greater for eve2:neutral. eve2:wt drove greater transcription than eve2:neutral, but it did so while activating, proportionally, more frequent short lifetimes.

The biexponential nature of the active transcription lifetimes was unexpected. We hypothesized that this reflects a change of the gene regulatory network over time, and therefore, characteristically longer active lifetimes only occur early in NC 14. To test this, we divided the active lifetime measurements of Figure 3B into two subsets: those that first activated early in NC 14 and those that first activated later (Figures 3C and S7, respectively; see STAR Methods). We applied the model in Equation 2 to each of the two subset distributions (early and later) of eve2:wt and eve2:neutral. These subsets yielded characteristic lifetimes, τ_1 and τ_2 , similar to those of the whole distributions (Table 2). However, the relative amplitudes, A and 1 - A, were different. In each case, the relative amplitude for the early distribution was dominated by long-lived activations (i.e., (1 - A) > A). For eve2:wt, the amplitude of longlived activations for the early distribution was $1 - A^{eve2:wt,early} =$ 0.52 ± 0.10 , up from $1 - A^{eve2:wt} = 0.29 \pm 0.05$ for the whole distribution. For eve2:neutral, the long-lived amplitude was $1 - A^{eve2:neutral,early} = 1.00 \pm 0.12$ for the early subset, compared with 1 - $A^{eve2:neutral} = 0.57 \pm 0.12$ for the whole distribution. The biexponential nature of these distributions cannot entirely be attributed to a hand-off between gene regulatory networks over the course of NC 14 (see discussion).

We determined how additional activities of Zld, Bcd, and Dstat in the TF reporters affected the characteristic active lifetimes by applying the model in Equation 2 to their respective distributions (Figure 3B). This revealed that only eve2[Dst]:neutral displayed active lifetime kinetics that were different from eve2:neutral (Table 2). Most notably, eve2[Dst]:neutral induced longer long-lived active times ($\tau_2^{eve2[Dst]}$:neutral). When these distributions were divided into early and later subsets, this trend held up for the later active lifetime distributions (Figure S7; Table 2). However, for the subset of early active times, all three activator reporters showed an increase in the characteristic lifetime for long-lived active times, τ_2 (Figure 3C; Table 2). Two conclusions can be drawn. First, the TF reporters increase active lifetimes by altering the long-lived characteristic time, τ_2 , and not the shortlived characteristic time, τ_1 , nor the fraction of long-lived events, 1 - A. Second, at any given time point during NC 14, more nuclei will be undergoing active transcription for each of the activating TF reporters compared with eve2:neutral. The modulation of the active transcription lifetime therefore meaningfully contributes to the differences in the dynamic transcription profiles of Figure 1D.



Idle transcription

We define idle transcription as the interval of time between the end of one observed active transcription interval and the beginning of the next within the same nucleus (Figures 3D, S8, and S9). During these intervals, the MCP-GFP transcription signal was below the detection threshold. Analogous to a car engine that idles while waiting at a stop light, transcription may still be occurring during these periods, but at a level that we could not detect. As with active transcription lifetimes, idle periods are related to the number of transcripts synthesized over NC 14; decreasing the idle period increases the total time over which a locus is actively transcribing. Modulating the length of idle periods in a time-dependent fashion can regulate when and how much of a transcript is produced.

We attempted to describe the idle period distributions with a kinetic model similar to the model that was used to describe the active transcription distributions (Figure S9). This attempt was unsuccessful but informative. Both the shape of the distributions (Figure S9B) and the model parameter values (Figure S9C) indicated that a single-exponential model was the best characterization of the data (explained in Figure S9). The characteristic time constant of a single-exponential distribution is the mean of that distribution. Accordingly, we chose to use the mean idle period to make comparisons.

The mean idle period is:

$$T^{i} = 1 / N^{i} \sum_{j=1}^{N^{i}} \frac{L_{j}^{i}}{n_{j}^{i}}$$
 (Equation 3)

Where N is the total number of nuclei with at least one detected active transcription interval, L is the cumulative length of time during which no transcription signal was detected in these same nuclei (see Figure S8), and n is the number of active transcription lifetimes (of any length) observed in these nuclei.

When considering the entirety of NC 14, the mean idle period increased for each of the TF reporters when compared with eve2:neutral (Figure 3E). These results likely do not represent meaningful biological conclusions; because eve2:neutral turns on transcription so late in the NC, there is little opportunity for long idle periods to occur before the onset of gastrulation (Figure S8). Thus, eve2:neutral drives short idle periods, and all TFs appear to increase idle periods in comparison. However, when analyzing idle periods that take place just after a nucleus turns on (see STAR Methods), eve2[Zld]:neutral showed a significant decrease in mean idle period relative to eve2:neutral, whereas eve2[Bcd]:neutral and eve2[Dst]:neutral showed no significant effects (Figure 3F).

DISCUSSION

Our goal was to determine the kinetic roles of three different TFs known to activate transcription in the *Drosophila* blastoderm embryo. We measured their effects on transcription in living embryos using a set of transcription reporters wherein the variants of *eve2* drive MCP-GFP marked nascent transcripts and contextualized our measurements using models derived from chemical kinetics. We characterized two bench-

mark reporters that served as effective lower and upper bounds for each measure of transcriptional activity, which allowed us to discern the effect of individual TFs by comparison. Straightforward inspection of the data yielded qualitative insights into roles for the three TFs: Zld, Bcd, and Dstat. Quantitative analysis with our empirical models provided additional insights by contrasting the probability distributions of first-passage activation times, active transcription lifetimes, and idle periods associated with each transgenic reporter. We found that the active transcription lifetime and mean idle period changed over time, with longer activation lifetimes and shorter idle periods early in the NC 14. We further found that each TF drove transcription in kinetically distinguishable ways, as summarized in Figure 4 and discussed in more detail below. Our results support the feasibility of kinetic synergy in eukaryotic gene regulation. Our results also highlight unresolved questions, including how TFs bound outside of canonical enhancers affect transcriptional output and how different combinations of TFs can achieve similar transcription outputs.

Insights into transcriptional kinetics

Inferring kinetic roles from dynamical data requires a mathematical model. To date, there are several examples of studies that use math models to describe MS2/MCP experiments (e.g., Eck et al., 30 Lammers et al., 40 and Zoller et al. 85). These models assumed a kinetic scheme, typically composed of two states, then attempted to measure transitions between or the probability of these states. This "forward theory" approach has the potential to realize the rate-limiting steps of regulation and will be essential to understanding how proteins and nucleic acids collectively give rise to transcription regulation.^{86,87} Unfortunately, these models are often phenomenological, given our lack of ability to directly measure most biochemical steps of eukaryotic transcription. "Reverse theory" (e.g., empirical theory), although lacking the predictive power of forward theory, nonetheless, has provided mechanistic insight into molecular interactions and regulatory concepts. Here, we argue that when the underlying kinetic scheme cannot be explicitly perturbed and may be "hideously complicated," an empirical approach makes "good sense."87 Although this approach contains certain assumptions, like any other, its power stems from a lack of assumptions about the underlying kinetics, mitigating concerns around the correctness of the model.

The models used here are agnostic to the underlying biochemical states of the transcriptional system. In effect, we are summarizing the kinetics of transcription signals by using empirical models to describe probability distributions. The time constants reported here are related, but not identical, to the underlying kinetic pathway of transcription. This is in contrast to other studies that have attempted to measure the kinetics of nascent transcription in embryos by using forward theory by assuming an underlying kinetic model. For example, Xu et al. assumed a two-state model of transcription, then extracted the rates between the states by fitting their model to distributions of nascent transcripts as measured in fixed embryos using single-molecule FISH.81 Lammers et al. also assumed an underlying two-state model, then measured transitions between them by inferring the state of the system from the intensity record of a fluorescent MS2/MCP reporter.40

Cell SystemsArticle



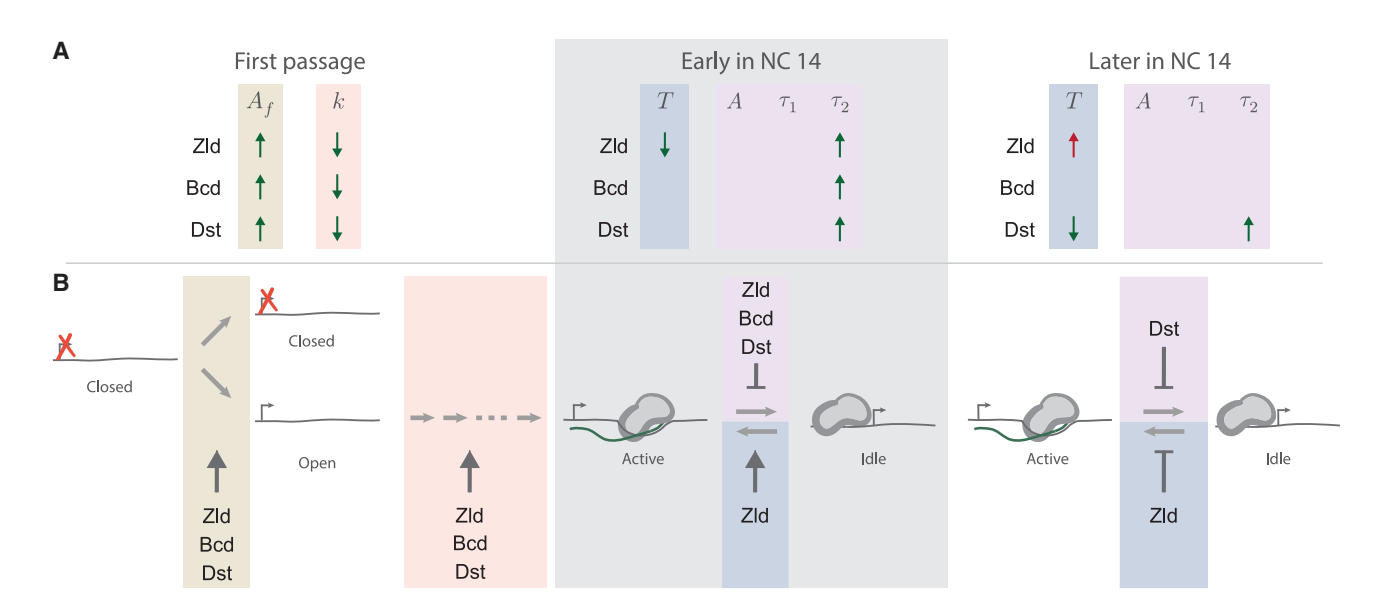


Figure 4. Kinetic roles of three transcriptional activators

(A) A graphical summary of the impact of each TF on each kinetic parameter. The arrows denote whether a parameter is increased or decreased by a TF. Parameter changes consistent with activation (i.e., lead to more transcription) are shown in green and changes consistent with repression in red. Beige and peach mark the first-passage transcription model parameters (Equation 1), blue marks the mean idle period (Equation 3), and purple the active transcription model parameters (Equation 2). The gray-shaded region denotes active and idle parameters early in NC 14.

(B) Model of transcription and its regulation during NC 14. Colored regions are as in (A). All three TFs increase the fraction of active nuclei (arrow in beige region), and they decrease the number of steps to first-passage transcription (arrow in peach region). At different times during NC 14, the TFs promote active transcription by suppressing the transition from the active to the idle state (T-bars in purple regions). Early in NC 14, Zld increases transcription by increasing the rate into the active state from the idle state, while Dst does so later (arrows in blue regions). Zld decreases this same rate later in the NC 14 (T-bar in blue region). The ellipsis represents a variable number of rate-limiting steps on the pathway to first-passage transcription.

In this work, we sought to quantify how dynamic transcriptional outputs changed with increased Zld, Bcd, and Dstat activities; our goal was to ask whether these three TFs had kinetically distinguishable roles. This goal had the advantage of not requiring any assumptions about the kinetic scheme *a priori*. It only requires precisely characterizing differences in transcriptional outputs. Our approach has well-established methods for its application^{74,88} and relies on a simple binarization of MS2/MCP data (STAR Methods). It is broadly applicable to all live imaging transcription studies.

Our analysis was restricted to the distributions of first-passage activation times, active transcription lifetimes, and idle periods. Other distributions, including fluorescence intensity (signal brightness) and intensity fluctuations (noise), were not included due to the dependency of these measurements on experimental conditions that are difficult to control. These include excitation laser drift and day-to-day variability, heterogeneous illumination across the field of view of the microscope, nucleus-to-nucleus variation in the depth of the reporter gene relative to the surface of the embryo, and photobleaching of GFP fluorophores over the course of an experiment. All of these sources of extrinsic noise bias fluorescence intensity measurements must be accounted for when reporting those distributions. These variables can and should be controlled to the extent that they can be (e.g., Figure S1). However, because we largely eschew measures of signal intensity, the approach laid out here is robust against them.

One notable result from this study is the large differences in the time delays between the end of anaphase and the first detection

of transcription (Figure 2). These differences strongly suggest that the regulation of the rates of first-passage transcription is an important and widespread mechanism of activating TFs. From qualitative inspection, each of the activating TFs reduced this delay, and they did so dramatically (Figure 1D). Our modeling approach further supported this observation and showed that each TF increased the active fraction of nuclei, which had previously been shown to be important for patterning in the embryo. 40,67 In addition, our model showed that each TF also decreased the number of rate-limiting steps, k. It is worth noting that these data are also consistent with a model, wherein each TF lowers the time constant of each of several consecutive rate-limiting steps (this can be shown by globally fitting k while fitting τ_0 to each construct individually, see STAR Methods). In either case, each TF is implicated in regulating the kinetic steps that lead to the onset of transcription and not just the likelihood that a locus ever turns on.

To our knowledge, this is the second report of a biexponential probability distribution of active lifetime MS2/MCP measurements. Darzacq et al., using photoactivated MS2/MCP in cultured human cells, reported characteristic time constants (~33 and 250 s) of the same order of magnitude as those we report here. ⁸⁹ As noted above, this implies that two stable states of the system exist. However, what, biologically, these two stable states represent is not clear.

The short time constants reported here, τ_1 , match well to the time we predict a RNA Pol II molecule to process along the reporter gene used in these experiments. Recent reports of RNA Pol II elongation rates in the fly blastoderm range from 40 to



|--|

		T
All periods	eve2:neutral	89 ± 8 s
	eve2:wt	$152 \pm 7 s$
	eve2[Zld]:neutral	$176 \pm 9 s$
	eve2[Bcd]:neutral	$149 \pm 10 s$
	eve2[Dst]:neutral	$108 \pm 5 s$
Early periods	eve2:neutral	$41 \pm 7 s$
	eve2:wt	$45 \pm 4 s$
	eve2[Zld]:neutral	$24 \pm 3 s$
	eve2[Bcd]:neutral	$38 \pm 5 s$
	eve2[Dst]:neutral	$46 \pm 5 s$
Later periods	eve2:neutral	$81 \pm 6 s$
	eve2:wt	$159 \pm 7 s$
	eve2[Zld]:neutral	$183 \pm 10 s$
	eve2[Bcd]:neutral	155 ± 11 s
	eve2[Dst]:neutral	110 ± 6 s

See Equation 3. Early idle times are the first 20% detected for each reporter. Later idle times are the other 80%. Standard errors were computed using bootstrapping methods.

50 bp/s. 40,73 Here, the DNA template is \sim 3,400 bp from the end of the MS2 stem-loop cassette to the poly A termination signal. Assuming MCP-GFP binds quickly following the stem-loop synthesis and the nascent transcript is released quickly from the site of termination, a nascent transcript would be fluorescently tagged and colocalized with the gene locus for around 75 s. which is somewhat consistent with the τ_1 values reported here, 22-63 s. One interpretation supposes that the short-lived instances of transcription represent low-level stochastic initiation, wherein up to a handful of RNA Pol II molecules are able to initiate, elongate, and terminate together in succession before the initiation is once again ceased. The frequency and duration of these instances are minimally affected by TFs in this context.

Significant differences between the active lifetime distributions were almost entirely attributable to the changes in the long-lived characteristic lifetime, τ_2 (Figure 3B; Table 2). This parameter ranges from 140 to 600 s, which is longer than the \sim 75 s we might expect for the synthesis of a single transcript. During elongation, RNA Pol II processes at highly variable rates⁹⁰ and can enter paused states far downstream of the promoter.91 It is possible that these mechanisms lead to RNA Pol II traffic jams on the gene, leaving fluorescently tagged elongation complexes paused or arrested at the gene. The long-lived state that we observed may represent these instances, as was proposed by Darzacq et al.⁸⁹ In our data, each TF, at one time or another, dramatically increased the long-lived transcription lifetimes (Figure 4), suggesting the long-lived state represents a highly regulated state/s, wherein many RNA Pol II molecules successively initiate transcription and process over a time window lasting several hundred seconds.

This work also showed that a stripe enhancer, eve2, isolated from the other enhancers in the eve locus loses the ability to drive expressions as NC 14 progresses (Figure 1D, gray curve), despite the fact that the TFs that regulate eve2 remain present. This type of "enhancer shutdown" is widespread in the develop-

mental networks; many developmental genes are controlled by multiple enhancers (often called shadow enhancers) and the regulation of these genes can transition from one enhancer to another as the development progresses (e.g., Scholes et al. 61 and Dunipace et al. 92). In the *Drosophila* embryo, there are three different gene regulatory networks active over NC 14 that drive expressions of the seven pair-rule genes, including eve. The transition between these gene regulatory networks is marked by a change in the enhancer dependence. 93 However, the mechanisms of enhancer shutdown and/or hand-off between enhancers are not currently known. Our modeling revealed that the kinetic role of a TF can change over time (Figure 4), and we speculate that mechanisms of enhancer shutdown are related to the changing roles of TFs at individual genes. For example, some TFs initially have kinetic roles that lead to greater transcription, whereas later, they have roles that lead to reduced transcription, as discussed below. Exploring this process of enhancer shutdown is poised to be an emerging topic in developmental biology.

Insights into TF function

Zld is thought to act as a pioneer factor in the embryo, opening chromatin and maintaining it in a state competent for transcription. 94-96 Kinetically, it is reasonable to hypothesize that this mechanism would decrease the number of rate-limiting steps to first-passage transcription. Consistent with this, we found that in this context, Zld dramatically decreased the number of steps, k. However, Zld also affected other kinetic parameters (Figure 4). Zld increased the transcription by increasing the active transcription lifetimes, τ_2 , but only for early times in the NC. In addition, Zld increased the transcription early in the NC by decreasing the idle period, T(Table 3). Zld has been shown to perform multiple roles at different target genes, 30,33 but to our knowledge, this is the first evidence that it plays multiple roles at a single gene over time.

Two Zld binding site insertions served to turn the dynamic transcription profile of eve2:neutral into something close to that of eve2:wt (Figure 1D). From this qualitative observation, one might conclude that the similarity is due to a similar number of Zld binding motifs in both eve2[Zld]:neutral and eve2:wt (see the sequence schematics in Figure 1A), although regulatory sequences can be sensitive to binding motif position, orientation, and neighboring sequences.^{56,97} However, our modeling does not support this interpretation. Following the first passage into active transcription, eve2:wt maintained active transcription by increasing the active transcription lifetimes, τ_2 , relative to eve2:neutral over all of NC 14. Zld did so by increasing τ_2 and decreasing the mean idle period, but only for early times in the NC. Zld then repressed transcription later on by increasing idle periods in nuclei that were previously active. Therefore, the similarity between the eve2[Zld]:neutral and eve2:wt dynamic transcription profiles cannot entirely be attributed to Zld activity as the two regulatory sequences produce similar spatiotemporal outputs by acting on different combinations of kinetic parameters.

Bcd is a highly studied TF, with considerable focus placed on how the Bcd gradient and cooperative interactions between Bcd proteins regulate target genes. 44,45,48,98–100 Our characterization of kinetic roles found that Bcd, in this context, increased the



active fraction of nuclei and decreased the number of ratelimiting steps to first-passage transcription. This is, perhaps, consistent with a previous report of Bcd activity early in the NC and its capacity for pioneering activity. 98 However, early in the NC, Bcd displayed both activating and repressing kinetic roles by suppressing both the transition out of the active state as well as the transition into it (Figure 4). Later in the NC, Bcd had no significant impact on the kinetics of transcription. This may be unsurprising, given another report that Bcd is a bifunctional TF in certain contexts, 101 but the activating/repressing activities of Bcd reported here are different than the bifunctional regulation previously reported. In this work, Bcd acts to tune different parameters at different times during the NC, sometimes resulting in an increase in the number of transcripts synthesized, and other times, resulting in a decrease. Although intriguing, these conclusions should be treated with caution. In this work, the effect of additional Bcd motifs was relatively small. Of the three activating TF reporters, the dynamic transcription profile of eve2[Bcd]: neutral was most similar to the baseline profile of eve2:neutral (Figure 1D). This was to be expected for two reasons. First, Bcd has been characterized as a weak activator. 46,47 Second. of the three TFs tested here, eve2 contains the most native binding motif sequences for Bcd (Figure 1A). Therefore, Bcd activity may already be close to saturation. An alternative variant of the eve2 reporter with fewer Bcd binding sites may test this hypothesis and give further insights into the kinetic role of Bcd.

Dstat is ubiquitously expressed in the embryo, is known to activate even-skipped stripe 3 and 5,51,102,103 and is thought to activate all even-skipped enhancers. 78 There are two predicted binding motifs in eve2 and four, albeit weaker, predicted sites in the endogenous spacer sequence (Figure 1A). Given this, it was somewhat surprising that eve2[Dst]:neutral drove a dynamic transcription profile that differed starkly from both eve2:neutral and eve2:wt. In this context, Dstat exclusively displayed the kinetic roles that were consistent with increasing transcription (Figure 4). These results establish a role for Dstat during the initial activation of a locus: increasing the active fraction of nuclei and decreasing the number of rate-limiting steps to first-passage transcription. In addition, unlike both Bcd and Zld, Dstat activated transcription throughout NC 14 by increasing active lifetimes.

Finally, we acknowledge the temptation to generalize the kinetic role for these three TFs and state clearly that we do not claim to do so. Our data show that these TFs can perform kinetically distinguishable roles, in the limited context we explore here. This addresses our question about the plausibility of kinetic synergy and supports the idea that TFs could be characterized by their kinetic role. It may be that these TFs play these same kinetic roles in different contexts, consistent with the billboard model of enhancers. 104 However, TFs are known to exhibit strong context dependencies. It remains to be seen whether these roles are maintained across contexts, such as in different binding site configurations or when embedded in different enhancer contexts. Exploring how consistent a TF's kinetic role is across contexts is a worthy goal for future work.

Conclusions

A mandate of systems biology with respect to transcriptional regulation is to decipher the logic of transcriptional control and predict regulatory sequence function. 105 This requires establishing why specific TFs have been selected to operate at a particular gene at a particular time. We wondered whether the way each TF activates transcription is part of the answer. TF mechanisms have always been defined by the methods with which we characterize them. Genetic approaches establish proteins as activating or repressing, biochemistry identifies the complexes a protein interacts with, and genomics establishes the genetic targets of a protein. Each approach plays a role in unveiling the mechanisms by which TFs regulate transcription. A niche of live imaging-by MS2/MCP and other methods-is to define the kinetic mechanisms of regulation. The shortcoming of this approach is its scalability. It is difficult to imagine applying this approach to, for example, the hundreds of human TFs. 13 This is, however, a tractable task within the blastoderm with its ~40 TFs present, ¹⁰⁶ once again placing the blastoderm as a model for higher organisms.²⁸

The results presented here complicate conventional mechanistic labels for TFs such as activators, repressors, pioneer factors, and bifunctional factors. In this instance, Bcd and Zld act to unequivocally increase transcriptional outputs, but they do so by both activating some kinetic steps while repressing others (Figure 4). Does this make them activators or bifunctional factors? Each TF plays a significant role during the first-passage activation. Does this qualify each of them as a pioneer factor? Zld has a complicated kinetic role throughout the NC that includes more than what might reasonably be attributed to a pioneer factor. Defining TFs by their kinetic roles skirts these ambiguities. It builds on a foundation with which we can work toward predicting transcriptional outputs a priori.

STAR*METHODS

Detailed methods are provided in the online version of this paper and include the following:

- KEY RESOURCES TABLE
- RESOURCE AVAILABILITY
 - Lead contact
 - Materials availability
 - O Data and code availability
- EXPERIMENTAL MODEL AND SUBJECT DETAILS
 - Drosophila lines
- METHOD DETAILS
 - Cloning and transgenesis
 - Live imaging
 - Image analysis
- QUANTIFICATION AND STATISTICAL ANALYSIS
 - Determining model parameters
 - Error analysis

SUPPLEMENTAL INFORMATION

Supplemental information can be found online at https://doi.org/10.1016/j. cels.2023.03.006.

ACKNOWLEDGMENTS

We thank Tally Lambert and Jennifer Waters at The Nikon Imaging Center at Harvard Medical School for guiding the microscopy experiments, assistance



Cell Systems Article

in data processing, and lively discussions. We also thank Larry Friedman, Jane Kondev, members of the DePace lab, and our reviewers for helpful comments and feedback. This work was supported by the National Institutes of Health (grants 1F32GM128310, R01GM122928, and U01GM103804), the National Science Foundation (grants IOS-1452557 and 1715184), and grants from the Mckenzie Family Charitable Trust, the Lynch Foundation, the Giovanni Armenise-Harvard Foundation, and the Harriet Sugar Toibin Charitable Gift Annuity.

AUTHOR CONTRIBUTIONS

All authors designed the research. T.T.H. and B.J.V. performed the research. T.T.H. analyzed the data and drafted the manuscript. All authors contributed to writing the final version of the manuscript.

DECLARATION OF INTERESTS

A.H.D. is a member of the advisory board of Cell Systems.

INCLUSION AND DIVERSITY

One or more of the authors of this paper self-identifies as a member of the LGBTQIA+ community

Received: March 8, 2021 Revised: June 26, 2022 Accepted: March 21, 2023 Published: April 19, 2023

REFERENCES

- Stampfel, G., Kazmar, T., Frank, O., Wienerroither, S., Reiter, F., and Stark, A. (2015). Transcriptional regulators form diverse groups with context-dependent regulatory functions. Nature 528, 147–151.
- Scholes, C., DePace, A.H., and Sánchez, Á. (2016). Combinatorial gene regulation through kinetic control of the transcription cycle. Cell Syst. 4. 1–12.
- Herschlag, D., and Johnson, F.B. (1993). Synergism in transcriptional activation: a kinetic view. Genes Dev. 7, 173–179.
- 4. Johnson, A.D. (1995). The price of repression. Cell 81, 655-658.
- Workman, J.L., and Buchman, A.R. (1993). Multiple functions of nucleosomes and regulatory factors in transcription. Trends Biochem. Sci. 18, 90–95.
- Hughes, T.R. (2011). A Handbook of Transcription Factors (Springer Science & Business Media).
- Zaret, K.S., and Carroll, J.S. (2011). Pioneer transcription factors: establishing competence for gene expression. Genes Dev. 25, 2227–2241.
- 8. Gray, S., and Levine, M. (1996). Transcriptional repression in development. Curr. Opin. Cell Biol. 8, 358–364.
- Courey, A.J., and Jia, S. (2001). Transcriptional repression: the long and the short of it. Genes Dev. 15, 2786–2796.
- Majello, B., De Luca, P., and Lania, L. (1997). Sp3 is a bifunctional transcription regulator with modular independent activation and repression domains. J. Biol. Chem. 272, 4021–4026.
- Papatsenko, D., and Levine, M.S. (2008). Dual regulation by the Hunchback gradient in the Drosophila embryo. Proc. Natl. Acad. Sci. USA 105, 2901–2906.
- Duarte, F.M., Fuda, N.J., Mahat, D.B., Core, L.J., Guertin, M.J., and Lis, J.T. (2016). Transcription factors GAF and HSF act at distinct regulatory steps to modulate stress-induced gene activation. Genes Dev. 30, 1731–1746.
- Lambert, S.A., Jolma, A., Campitelli, L.F., Das, P.K., Yin, Y., Albu, M., Chen, X., Taipale, J., Hughes, T.R., and Weirauch, M.T. (2018). The human transcription factors. Cell 175, 598–599.
- Browning, D.F., and Busby, S.J.W. (2016). Local and global regulation of transcription initiation in bacteria. Nat. Rev. Microbiol. 14, 638–650.

- Friedman, L.J., and Gelles, J. (2012). Mechanism of transcription initiation at an activator-dependent promoter defined by single-molecule observation. Cell 148, 679–689.
- Harden, T.T., Wells, C.D., Friedman, L.J., Landick, R., Hochschild, A., Kondev, J., and Gelles, J. (2016). Bacterial RNA polymerase can retain σ 70 throughout transcription. Proc. Natl. Acad. Sci. USA 113, 602–607.
- Bae, B., Feklistov, A., Lass-Napiorkowska, A., Landick, R., and Darst, S.A. (2015). Structure of a bacterial RNA polymerase holoenzyme open promoter complex. eLife 4, 1–23.
- Chen, J., Chiu, C., Gopalkrishnan, S., Chen, A.Y., Olinares, P.D.B., Saecker, R.M., Winkelman, J.T., Maloney, M.F., Chait, B.T., Ross, W., et al. (2020). Stepwise promoter melting by bacterial RNA polymerase. Mol. Cell 78, 275–288.e6.
- Villar, D., Flicek, P., and Odom, D.T. (2014). Evolution of transcription factor binding in metazoans mechanisms and functional implications. Nat. Rev. Genet. 15, 221–233.
- Guo, Z., Qin, J., Zhou, X., and Zhang, Y. (2018). Insect transcription factors: A landscape of their structures and biological functions in drosophila and beyond. Int. J. Mol. Sci. 19, 3691. https://doi.org/10.3390/ijms19113691.
- Lis, J.T. (2019). A 50 year history of technologies that drove discovery in eukaryotic transcription regulation. Nat. Struct. Mol. Biol. 26, 777–782.
- Fazal, F.M., Meng, C.A., Murakami, K., Kornberg, R.D., and Block, S.M. (2015). Real-time observation of the initiation of RNA polymerase II transcription. Nature 525, 274–277.
- Rosen, G.A., Baek, I., Friedman, L.J., Joo, Y.J., Buratowski, S., and Gelles, J. (2020). Dynamics of RNA polymerase II and elongation factor Spt4/5 recruitment during activator-dependent transcription. Proc. Natl. Acad. Sci. USA 117, 32348–32357. https://doi.org/10.1073/pnas.2011224117.
- 24. Chen, H., and Larson, D.R. (2016). What have single-molecule studies taught us about gene expression? Genes Dev. 30, 1796–1810.
- Lim, B. (2018). Imaging transcriptional dynamics. Curr. Opin. Biotechnol. 52, 49–55.
- Bentovim, L., Harden, T.T., and DePace, A.H. (2017). Transcriptional precision and accuracy in development: from measurements to models and mechanisms. Development 144, 3855–3866.
- Lenstra, T.L., Rodriguez, J., Chen, H., and Larson, D.R. (2016).
 Transcription dynamics in living cells. Annu. Rev. Biophys. 45, 25–47.
- Gregor, T., Garcia, H.G., and Little, S.C. (2014). The embryo as a laboratory: quantifying transcription in Drosophila. Trends Genet. 30, 364–375.
- Bothma, J.P., Norstad, M.R., Alamos, S., and Garcia, H.G. (2018).
 LlamaTags: A versatile tool to image transcription factor dynamics in live embryos. Cell 173, 1810–1822.e16.
- Eck, E., Liu, J., Kazemzadeh-Atoufi, M., Ghoreishi, S., Blythe, S.A., and Garcia, H.G. (2020). Quantitative dissection of transcription in development yields evidence for transcription-factor-driven chromatin accessibility. eLife 9, e56429. https://doi.org/10.7554/eLife.56429.
- Keller, S.H., Jena, S.G., Yamazaki, Y., and Lim, B. (2020). Regulation of spatiotemporal limits of developmental gene expression via enhancer grammar. Proc. Natl. Acad. Sci. USA 117, 15096–15103.
- **32.** Yamada, S., Whitney, P.H., Huang, S.K., Eck, E.C., Garcia, H.G., and Rushlow, C.A. (2019). The drosophila pioneer factor Zelda modulates the nuclear microenvironment of a dorsal target enhancer to potentiate transcriptional output. Curr. Biol. *29*, 1387–1393.e5.
- Dufourt, J., Trullo, A., Hunter, J., Fernandez, C., Lazaro, J., Dejean, M., Morales, L., Nait-Amer, S., Schulz, K.N., Harrison, M.M., et al. (2018). Temporal control of gene expression by the pioneer factor Zelda through transient interactions in hubs. Nat. Commun. 9, 5194.
- Fernandez, C., and Lagha, M. (2019). Lighting up gene activation in living drosophila embryos. In Imaging Gene Expression: Methods and Protocols, Y. Shav-Tal, ed. (Springer), pp. 63–74.
- Wissink, E.M., Vihervaara, A., Tippens, N.D., and Lis, J.T. (2019). Nascent RNA analyses: tracking transcription and its regulation. Nat. Rev. Genet. 20, 705–723.

Article



- Fukaya, T., Lim, B., and Levine, M. (2016). Enhancer control of transcriptional bursting. Cell 166, 358–368.
- Bothma, J.P., Garcia, H.G., Ng, S., Perry, M.W., Gregor, T., and Levine, M. (2015). Enhancer additivity and non-additivity are determined by enhancer strength in the Drosophila embryo. eLife 4, 1–14.
- Desponds, J., Tran, H., Ferraro, T., Lucas, T., Perez Romero, C., Guillou, A., Fradin, C., Coppey, M., Dostatni, N., and Walczak, A.M. (2016). Precision of Readout at the hunchback Gene: analyzing Short Transcription Time Traces in Living Fly Embryos. PLoS Comput. Biol. 12, e1005256.
- Desponds, J., Vergassola, M., and Walczak, A.M. (2020). A mechanism for hunchback promoters to readout morphogenetic positional information in less than a minute. eLife 9, e49758. https://doi.org/10.7554/ eLife.49758.
- Lammers, N.C., Galstyan, V., Reimer, A., Medin, S.A., Wiggins, C.H., and Garcia, H.G. (2020). Multimodal transcriptional control of pattern formation in embryonic development. Proc. Natl. Acad. Sci. USA 117, 836–847.
- Staudt, N., Fellert, S., Chung, H.-R., Jäckle, H., and Vorbrüggen, G. (2006). Mutations of the Drosophila zinc finger-encoding gene vielfältig impair mitotic cell divisions and cause improper chromosome segregation. Mol. Biol. Cell 17, 2356–2365.
- Harrison, M.M., and Eisen, M.B. (2015). Transcriptional Activation of the Zygotic Genome in Drosophila, First Edition (Elsevier Inc.).
- McGregor, A.P. (2005). How to get ahead: the origin, evolution and function of bicoid. BioEssays 27, 904–913.
- Struhl, G., Struhl, K., and Macdonald, P.M. (1989). The gradient morphogen bicoid is a concentration-dependent transcriptional activator. Cell 57, 1259–1273.
- Burz, D.S., Rivera-Pomar, R., Jäckle, H., and Hanes, S.D. (1998).
 Cooperative DNA-binding by bicoid provides a mechanism for threshold-dependent gene activation in the Drosophila embryo. EMBO J. 17, 5998–6009.
- Ma, X., Yuan, D., Scarborough, T., and Ma, J. (1999). Contributions to gene activation by multiple functions of bicoid. Biochem. J. 338, 447–455.
- Ma, X., Yuan, D., Diepold, K., Scarborough, T., and Ma, J. (1996). The Drosophila morphogenetic protein bicoid binds DNA cooperatively. Development 122, 1195–1206.
- Park, J., Estrada, J., Johnson, G., Vincent, B.J., Ricci-Tam, C., Bragdon, M.D., Shulgina, Y., Cha, A., Wunderlich, Z., Gunawardena, J., et al. (2019). Dissecting the sharp response of a canonical developmental enhancer reveals multiple sources of cooperativity. eLife 8, e41266. https://doi.org/10.7554/eLife.41266.
- Herrera, S.C., and Bach, E.A. (2019). JAK/STAT signaling in stem cells and regeneration: from Drosophila to vertebrates. Development 146, dev167643. https://doi.org/10.1242/dev.167643.
- Tsurumi, A., Xia, F., Li, J., Larson, K., LaFrance, R., and Li, W.X. (2011).
 STAT is an essential activator of the zygotic genome in the early drosophila embryo. PLoS Genet. 7, e1002086. https://doi.org/10.1371/journal.pgen.1002086.
- Yan, R., Small, S., Desplan, C., Dearolf, C.R., and Darnell, J.E., Jr. (1996).
 Identification of a Stat gene that functions in Drosophila development.
 Cell 84. 421–430.
- Barr, K.A., Martinez, C., Moran, J.R., Kim, A.-R., Ramos, A.F., and Reinitz, J. (2017). Synthetic enhancer design by in silico compensatory evolution reveals flexibility and constraint in cis-regulation. BMC Syst. Biol. 11, 116.
- Small, S., Blair, A., and Levine, M. (1992). Regulation of even-skipped stripe 2 in the Drosophila embryo. EMBO J. 11, 4047–4057.
- Arnosti, D.N., Barolo, S., Levine, M., and Small, S. (1996). The eve stripe 2 enhancer employs multiple modes of transcriptional synergy. Development 122, 205–214.

- Goto, T., Macdonald, P., and Maniatis, T. (1989). Early and late periodic patterns of even skipped expression are controlled by distinct regulatory elements that respond to different spatial cues. Cell 57, 413–422.
- Vincent, B.J., Estrada, J., and DePace, A.H. (2016). The appeasement of Doug: a synthetic approach to enhancer biology. Integr. Biol. 8, 475–484.
- Berrocal, A., Lammers, N.C., Garcia, H.G., and Eisen, M.B. (2020).
 Kinetic sculpting of the seven stripes of the Drosophila even-skipped gene. eLife 9, e61635. https://doi.org/10.7554/eLife.61635.
- Lim, B., Fukaya, T., Heist, T., and Levine, M. (2018). Temporal dynamics of pair-rule stripes in living Drosophila embryos. Proc. Natl. Acad. Sci. USA 115, 8376–8381.
- Bothma, J.P., Garcia, H.G., Esposito, E., Schlissel, G., Gregor, T., and Levine, M. (2014). Dynamic regulation of eve stripe 2 expression reveals transcriptional bursts in living Drosophila embryos. Proc. Natl. Acad. Sci. USA 111, 10598–10603.
- Estrada, J., Ruiz-Herrero, T., Scholes, C., Wunderlich, Z., and DePace, A.H. (2016). SiteOut: an online tool to design binding site-free DNA sequences. PLoS One 11, e0151740.
- Scholes, C., Biette, K.M., Harden, T.T., and DePace, A.H. (2019). Signal integration by shadow enhancers and enhancer duplications varies across the drosophila embryo. Cell Rep. 26, 2407–2418.e5.
- **62.** Weingarten-Gabbay, S., and Segal, E. (2014). The grammar of transcriptional regulation. Hum. Genet. *133*, 701–711.
- Hocine, S., Raymond, P., Zenklusen, D., Chao, J.A., and Singer, R.H. (2013). Single-molecule analysis of gene expression using two-color RNA labeling in live yeast. Nat. Methods 10, 119–121.
- Groth, A.C., Fish, M., Nusse, R., and Calos, M.P. (2004). Construction of transgenic Drosophila by using the site-specific integrase from phage phiC31. Genetics 166, 1775–1782.
- 65. Wu, Y., Wawrzusin, P., Senseney, J., Fischer, R.S., Christensen, R., Santella, A., York, A.G., Winter, P.W., Waterman, C.M., Bao, Z., et al. (2013). Spatially isotropic four-dimensional imaging with dual-view plane illumination microscopy. Nat. Biotechnol. 31, 1032–1038.
- Zoller, B., Little, S.C., and Gregor, T. (2018). Diverse spatial expression patterns emerge from unified kinetics of transcriptional bursting. Cell 175, 835–847.e25.
- 67. Garcia, H.G., Tikhonov, M., Lin, A., and Gregor, T. (2013). Quantitative imaging of transcription in living Drosophila embryos links polymerase activity to patterning. Curr. Biol. 23, 2140–2145.
- Lucas, T., Ferraro, T., Roelens, B., De Las Heras Chanes, J., Walczak, A.M., Coppey, M., and Dostatni, N. (2013). Live imaging of bicoid-dependent transcription in Drosophila embryos. Curr. Biol. 23, 2135–2139.
- Laissue, P.P., Alghamdi, R.A., Tomancak, P., Reynaud, E.G., and Shroff, H. (2017). Assessing phototoxicity in live fluorescence imaging. Nat. Methods 14, 657–661.
- Jemielita, M., Taormina, M.J., Delaurier, A., Kimmel, C.B., and Parthasarathy, R. (2013). Comparing phototoxicity during the development of a zebrafish craniofacial bone using confocal and light sheet fluorescence microscopy techniques. J. Biophotonics 6, 920–928.
- Icha, J., Weber, M., Waters, J.C., and Norden, C. (2017). Phototoxicity in live fluorescence microscopy, and how to avoid it. BioEssays 39. https:// doi.org/10.1002/bies.201700003.
- Bertrand, E., Chartrand, P., Schaefer, M., Shenoy, S.M., Singer, R.H., and Long, R.M. (1998). Localization of ASH1 mRNA particles in living yeast. Mol. Cell 2, 437–445.
- Fukaya, T., Lim, B., and Levine, M. (2017). Rapid rates of Pol II elongation in the drosophila embryo. Curr. Biol. 27, 1387–1391.
- Friedman, L.J., and Gelles, J. (2015). Multi-wavelength single-molecule fluorescence analysis of transcription mechanisms. Methods 86, 27–36.
- Janssens, H., Hou, S., Jaeger, J., Kim, A.-R., Myasnikova, E., Sharp, D., and Reinitz, J. (2006). Quantitative and predictive model of transcriptional control of the Drosophila melanogaster even skipped gene. Nat. Genet. 38, 1159–1165.



Cell Systems Article

- Staller, M.V., Vincent, B.J., Bragdon, M.D.J., Lydiard-Martin, T., Wunderlich, Z., Estrada, J., and DePace, A.H. (2015). Shadow enhancers enable Hunchback bifunctionality in the Drosophila embryo. Proc. Natl. Acad. Sci. USA 112, 785–790.
- Vincent, B.J., Staller, M.V., Lopez-Rivera, F., Bragdon, M.D.J., Pym, E.C.G., Biette, K.M., Wunderlich, Z., Harden, T.T., Estrada, J., and DePace, A.H. (2018). Hunchback is counter-repressed to regulate even-skipped stripe 2 expression in Drosophila embryos. PLoS Genet. 14, e1007644.
- Barr, K.A., and Reinitz, J. (2017). A sequence level model of an intact locus predicts the location and function of nonadditive enhancers. PLoS One 12, e0180861.
- Parsons, G.G., and Spencer, C.A. (1997). Mitotic repression of RNA polymerase II transcription is accompanied by release of transcription elongation complexes. Mol. Cell. Biol. 17, 5791–5802.
- Esposito, E., Lim, B., Guessous, G., Falahati, H., and Levine, M. (2016).
 Mitosis-associated repression in development. Genes Dev. 30, 1503–1508.
- Xu, H., Skinner, S.O., Sokac, A.M., and Golding, I. (2016). Stochastic kinetics of nascent RNA. Phys. Rev. Lett. 117, 128101. https://doi.org/10.1103/PhysRevLett.117.128101.
- 82. Lim, B., Heist, T., Levine, M., and Fukaya, T. (2018). Visualization of transvection in living drosophila embryos. Mol. Cell 70, 287–296.e6.
- Wunderlich, Z., Bragdon, M.D.J., Vincent, B.J., White, J.A., Estrada, J., and DePace, A.H. (2015). Krüppel expression levels are maintained through compensatory evolution of shadow enhancers. Cell Rep. 12, 1740–1747.
- Myong, S., Bruno, M.M., Pyle, A.M., and Ha, T. (2007). Spring-loaded mechanism of DNA unwinding by hepatitis C virus NS3 helicase. Science 317, 513–516.
- Zoller, B., Nicolas, D., Molina, N., and Naef, F. (2015). Structure of silent transcription intervals and noise characteristics of mammalian genes. Mol. Syst. Biol. 11, 823.
- 86. Phillips, R. (2015). Theory in Biology: Figure 1 or Figure 7? Trends Cell Biol. 25, 723–729.
- 87. Gunawardena, J. (2014). Models in biology: "accurate descriptions of our pathetic thinking.". BMC Biol. 12, 29.
- 88. Zhou, Y., and Zhuang, X. (2007). Kinetic analysis of sequential multistep reactions. J. Phys. Chem. B *111*, 13600–13610.
- Darzacq, X., Shav-Tal, Y., de Turris, V., Brody, Y., Shenoy, S.M., Phair, R.D., and Singer, R.H. (2007). In vivo dynamics of RNA polymerase II transcription. Nat. Struct. Mol. Biol. 14, 796–806.
- Tolić-Nørrelykke, S.F., Engh, A.M., Landick, R., and Gelles, J. (2004).
 Diversity in the rates of transcript elongation by single RNA polymerase molecules. J. Biol. Chem. 279, 3292–3299.
- 91. Landick, R. (2006). The regulatory roles and mechanism of transcriptional pausing. Biochem. Soc. Trans. *34*, 1062–1066.
- Dunipace, L., Saunders, A., Ashe, H.L., and Stathopoulos, A. (2013).
 Autoregulatory feedback controls sequential action of cis-regulatory modules at the Brinker locus. Dev. Cell 26, 536–543.
- Clark, E., and Akam, M. (2016). Odd-paired controls frequency doubling in Drosophila segmentation by altering the pair-rule gene regulatory network. eLife 5, e18215. https://doi.org/10.7554/eLife.18215.
- Harrison, M.M., Li, X.Y., Kaplan, T., Botchan, M.R., and Eisen, M.B. (2011).
 Zelda binding in the early Drosophila melanogaster embryo marks regions subsequently activated at the maternal-to-zygotic transition. PLoS Genet. 7, e1002266. https://doi.org/10.1371/journal.pgen.1002266.
- Sun, Y., Nien, C.Y., Chen, K., Liu, H.Y., Johnston, J., Zeitlinger, J., and Rushlow, C. (2015). Zelda overcomes the high intrinsic nucleosome barrier at enhancers during Drosophila zygotic genome activation. Genome Res. 25. 1703–1714.
- Schulz, K.N., Bondra, E.R., Moshe, A., Villalta, J.E., Lieb, J.D., Kaplan, T., McKay, D.J., and Harrison, M.M. (2015). Zelda is differentially required for chromatin accessibility, transcription-factor binding and gene expression in the early Drosophila embryo. Genome Res. 25, 1715–1726.

- Erceg, J., Saunders, T.E., Girardot, C., Devos, D.P., Hufnagel, L., and Furlong, E.E.M. (2014). Subtle changes in motif positioning cause tissue-specific effects on robustness of an enhancer's activity. PLoS Genet. 10, e1004060.
- 98. Hannon, C.E., Blythe, S.A., and Wieschaus, E.F. (2017). Concentration dependent chromatin states induced by the bicoid morphogen gradient. eLife 6, e28275. https://doi.org/10.7554/eLife.28275.
- Driever, W., and Nüsslein-Volhard, C. (1988). A gradient of bicoid protein in Drosophila embryos. Cell 54, 83–93.
- 100. Lebrecht, D., Foehr, M., Smith, E., Lopes, F.J.P., Vanario-Alonso, C.E., Reinitz, J., Burz, D.S., and Hanes, S.D. (2005). Bicoid cooperative DNA binding is critical for embryonic patterning in Drosophila. Proc. Natl. Acad. Sci. USA 102, 13176–13181.
- Liaw, G.J., and Lengyel, J.A. (1993). Control of tailless expression by bicoid, dorsal and synergistically interacting terminal system regulatory elements. Mech. Dev. 40, 47–61.
- Struffi, P., Corado, M., Kaplan, L., Yu, D., Rushlow, C., and Small, S. (2011). Combinatorial activation and concentration-dependent repression of the Drosophila even skipped stripe 3+7 enhancer. Development 138, 4291–4299.
- 103. Fujioka, M., Emi-Sarker, Y., Yusibova, G.L., Goto, T., and Jaynes, J.B. (1999). Analysis of an even-skipped rescue transgene reveals both composite and discrete neuronal and early blastoderm enhancers, and multistripe positioning by gap gene repressor gradients. Development 126, 2527–2538.
- 104. Arnosti, D.N., and Kulkarni, M.M. (2005). Transcriptional enhancers: intelligent enhanceosomes or flexible billboards? J. Cell. Biochem. 94, 890–898.
- Catarino, R.R., and Stark, A. (2018). Assessing sufficiency and necessity of enhancer activities for gene expression and the mechanisms of transcription activation. Genes Dev. 32, 202–223.
- 106. MacArthur, S., Li, X.-Y., Li, J., Brown, J.B., Chu, H.C., Zeng, L., Grondona, B.P., Hechmer, A., Simirenko, L., Keränen, S.V.E., et al. (2009). Developmental roles of 21 Drosophila transcription factors are determined by quantitative differences in binding to an overlapping set of thousands of genomic regions. Genome Biol. 10, R80.
- 107. Hare, E.E., Peterson, B.K., Iyer, V.N., Meier, R., and Eisen, M.B. (2008). Sepsid even-skipped enhancers are functionally conserved in Drosophila despite lack of sequence conservation. Perrimon N, editor. PLoS Genet 4, e1000106. PMID: 18584029. https://doi.org/10.1371/journal.pgen.1000106.
- 108. Gibson, D.G., Young, L., Chuang, R.-Y., Venter, J.C., Hutchison, C.A., 3rd, and Smith, H.O. (2009). Enzymatic assembly of DNA molecules up to several hundred kilobases. Nat. Methods 6, 343–345.
- 109. Fish, M.P., Groth, A.C., Calos, M.P., and Nusse, R. (2007). Creating transgenic Drosophila by microinjecting the site-specific phiC31 integrase mRNA and a transgene-containing donor plasmid. Nat. Protoc. 2, 2325–2331.
- 110. Markstein, M., Pitsouli, C., Villalta, C., Celniker, S.E., and Perrimon, N. (2008). Exploiting position effects and the gypsy retrovirus insulator to engineer precisely expressed transgenes. Nat. Genet. 40, 476–483.
- 111. Kumar, A., Wu, Y., Christensen, R., Chandris, P., Gandler, W., McCreedy, E., Bokinsky, A., Colón-Ramos, D.A., Bao, Z., McAuliffe, M., et al. (2014). Dual-view plane illumination microscopy for rapid and spatially isotropic imaging. Nat. Protoc. 9, 2555–2573.
- 112. Edelstein, A.D., Tsuchida, M.A., Amodaj, N., Pinkard, H., Vale, R.D., and Stuurman, N. (2014). Advanced methods of microscope control using μManager software. J. Biol. Methods 1, 1. https://doi.org/10.14440/ jbm.2014.36.
- 113. Ensign, D.L., and Pande, V.S. (2009). Bayesian single-exponential kinetics in single-molecule experiments and simulations. J. Phys. Chem. B 113, 12410–12423.
- 114. Efron, B., and Tibshirani, R.J. (1994). An Introduction to the Bootstrap (CRC Press).



STAR*METHODS

KEY RESOURCES TABLE

REAGENT or RESOURCE	SOURCE	IDENTIFIER
Experimental models: Organisms/strains		
yw; His2Av-mRFP1; MCP-NoNLS-eGFP	Garcia et al. ⁶⁷	N/A
y[1] w[67c23]; P{y[+t7.7]=CaryP}attP2	Bloomington Stock Center	RRID: BDSC_5253
y[1] w[67c23]; P{eve2:neutral}attP2	This study	Stock No. 750, eve2:neutral
y[1] w[67c23]; P{eve2:wt}attP2	This study	Stock No. 751, eve2:wt
y[1] w[67c23]; P{eve2[Zld]:neutral}attP2	This study	Stock No. 754, eve2[Zld]:neutral
y[1] w[67c23]; P{eve2[Bcd]:neutral}attP2	This study	Stock No. 753, eve2[Bcd]:neutral
y[1] w[67c23]; P{eve2[Dst]:neutral}attP2	This study	Stock No. 755, eve2[Dst]:neutral
Deposited data		
MS2 data – maximum projections	This study	https://doi.org/10.5281/zenodo.6313179, https://doi.org/10.5281/zenodo.6313548
MS2 data – data files	This study	https://doi.org/10.5281/zenodo.6554150
Software and algorithms		
MATLAB_R2019b	MathWorks	https://www.mathworks.com
Custom analysis scripts	This study	https://github.com/tth0603/flimscroll

RESOURCE AVAILABILITY

Lead contact

Further information and requests for resources and reagents should be directed to Angela DePace, angela_depace@hms. harvard.edu.

Materials availability

The plasmids generated in this study are available upon request.

The fly strains generated in this study are available upon request.

Data and code availability

All data have been deposited at Zenodo (In these archives, source data are provided as maximum projection images (https://doi.org/ 10.5281/zenodo.6313179 and https://doi.org/10.5281/zenodo.6313548) as well as data files (https://doi.org/10.5281/zenodo. 6554150) that can be read by the Matlab program and scripts that were used to generate these figures.) and are publicly available as of the date of publication. The DOI is listed in the key resources table.

All original code has been deposited at Github (https://github.com/tth0603/flimscroll) and is publicly available as of the date of publication. The DOI is listed in the key resources table.

Any additional information required to reanalyze the data reported in this paper is available from the lead contact upon request Source data for Figures 1B-1D, 2B, 3B, 3C, 3E, 3F, and S1-S9 are archived at https://zenodo.org. In these archives, source data are provided as maximum projection images (https://doi.org/10.5281/zenodo.6313179 and https://doi.org/10.5281/zenodo. 6313548) as well as data files (https://doi.org/10.5281/zenodo.6554150) that can be read by the Matlab program and scripts that were used to generate these figures. This archive contains an index that explains which images and data files belong to each experiment.

The Matlab scripts and program that were used to segment and track nuclei and spots of transcription, colocalize spots with nuclei, and analyze the subsequent data to produce figures are publicly available at https://github.com/tth0603/flimscroll.

EXPERIMENTAL MODEL AND SUBJECT DETAILS

Drosophila lines

Flies were raised on standard cornmeal-molasses-agar medium and grown at 25° C. The sex of the embryos used in this study was not determined.





METHOD DETAILS

Cloning and transgenesis

An MS2 transcription reporter gene was placed in the pBOY vector backbone (Hare et al. 107) using Gibson isothermal assembly. 108 The reporter consisted of the Drosophila melanogaster even-skipped core promoter, a 1295 bp sequence encoding 24 tandem repeats of MS2 stem loops (Hocine et al. 63; Addgene #45162), 3 kb of the lacZ gene, and the alpha-tubulin 3' UTR. For eve2:neutral, we computationally designed a sequence predicted to lack binding motifs for regulatory proteins active in patterning the blastoderm embryo, motifs for architectural binding proteins, and core promoter sequences using the online binding motif removal tool SiteOut. 60,61 This sequence, along with the 484 basepair minimal eve2 sequence, 53 was commercially synthesized (GenScript gene synthesis services) and cloned into our reporter plasmid through isothermal assembly. 108 For eve2:wt, the 1033 bp that separate minimal eve2 and the even-skipped promoter were PCR amplified from genomic DNA, then inserted into our reporter plasmid along with eve2 also using isothermal assembly. For eve2[Zld]:neutral, a sequence identical to eve2 save for two motif mutations-tccgccgat became tAATccgat at 299 bp with respect to the 5' end of eve2 and ttctgcggg became ttAATcCgg at 323 bp—was synthesized and cloned as above. For eve2[Bcd]:neutral, the mutations to eve2 were: tccgccgat became tcAgGTATt and ttctgcggg became ttcAgGTAg. For eve2[Dst]:neutral the mutations to eve2 were: tccgccgat became tTcCcGgaA and ttctgcggg became ttcCCGaAA.

We verified the sequence of the enhancers and promoter of all reporter constructs prior to injection, and checked the length of the MS2 cassette by restriction digest. The pBOY backbone contains an attB site for phiC31-mediated site-specific recombination 109 and a mini-white gene for transformant selection. For each construct, BestGene Inc. (Chino Hills, CA) injected midi-prepped DNA into 200 embryos of Bloomington Stock BL8622, which contains the attP2 landing site on chromosome 3L. 110 All constructs are integrated into this same attP2 landing site. After the constructs were successfully integrated into the fly genome, we prepared genomic DNA, PCR-amplified the transgene and repeated the sequencing and restriction digest verification of the reporters.

Live imaging

Virgin females with the genotype vw; His2Av-mRFP1; MCP-NoNLS-eGFP⁶⁷ were crossed to males homozygous for one of the transgenic transcription reporters. Embryos no older than 30 minutes were collected and subsequently dechorionated in freshly-made 50% bleach for two minutes. Embryos were placed on a single coverslip and bathed in Schneider's Drosophila medium (Gibco), where they remained for the entire duration of the experiment.

Light sheet microscopy was performed on a diSPIM (Applied Scientific Instrumentation, Eugene OR) setup as previously described, 111 though only a single imaging view was used for all experiments presented here. 488 & 561 nm laser lines from an Agilent laser launch were fiber-coupled into MEMS-mirror scanhead, used to create a virutally-swept light sheet. A pair of perpendicular water-dipping, long-working distance objectives (NIR APO 40×, 0.8 NA, Cat. No. MRD07420; Nikon, Melville, NY) were used to illuminate the sample and to collect the resulting fluorescence. All laser lines were reflected with a quad-pass ZT405/488/561/640rpcv2 dichroic and emission was selected with a ZET405/488/561/635M filter (Chroma) before detection on a sCMOS camera (ORCA Flash v2.0; Hamamatsu). For data acquisition and instrument control, we used the ASI diSPIM plugin within MicroManager. 112

To ensure consistent excitation laser power and light sheet shape from experiment to experiment, two laser power measurements were made prior to each acquisition. First, a power meter was used to set the 488 nm line to 650 ± 30 μW incident to the excitation scanner (see schematic in Kumar et al. 111). This ensured consistent excitation laser power. Next, to ensure the shape of the light sheet was the same for each experiment, we first determined the optimal light sheet shape at the 650 μW laser power. To do so, an iris within the excitation scanner was adjusted to maximize the width of the sheet at its waist (~8.0 µm). This created the optimal light sheet shape: an homogeneous sheet width across the microscope field of view and even excitation across the sample. This iris setting is coupled to the laser power exiting the excitation objective (incident to the sample). Thus, for the optimal light sheet shape, the laser power incident to the sample was measured. This value, $12 \pm 0.5 \,\mu\text{W}$, was then used to adjust the iris setting prior to each experiment to reproduce the shape of the light sheet. In this way, we attempted to create even excitation across the field of view that was consistent between acquisitions.

Image acquisition commenced during NC 13 and ceased at about the beginning of gastrulation, as judged by the directed movement of nuclei that marks the start of gastrulation. Z-stacks were acquired every 30 seconds (i.e. 2 exposures/minute; Figure S1) by sweeping the sheet in conjunction with the detection plane (controlled via piezo motor) through the sample. Z-stacks were composed of 80 Z-planes separated by 0.5 µm; the exposure time to collect a single Z-plane was 50 milliseconds. To ensure that each part of a sample within the imaging volume was exposed to a similar number of excitation photons, and that this value was the same in all experiments, the area of each Z-stack (i.e. the size of the field of view in the X- and Y-direction) was kept constant. The time required to acquire a single image stack was about 11.8 s.

Multiple embryos were imaged for each transgenic reporter. Because all distributions and modeling reported here relied on the assumption that each nucleus was an independent measurement, we aimed for a sufficient number of nuclei from each construct to ensure robust and reproducible distributions (i.e. first passage, active transcription, idle period distributions). For all constructs save for eve2:neutral, measurements from two embryos were sufficient to meet this criteria. Because of the smaller number of active nuclei in eve2:neutral, that condition required imaging four embryos to collect a number of measurements similar to those eve2:wt, eve2[Zld]:neutral, eve2[Bcd]:neutral, and eve2[Dst]:neutral. See Figure S4.



Image analysis

Image analysis was done using custom software implemented in MATLAB, see Data and Code Availability. Algorithms for automatic spot and nuclei detection and tracking were adapted from.⁷⁴ Following maximum intensity projection of mRFP1 and eGFP emission Z-stacks for each time frame, the nuclei were segmented. Spots of transcription were located in each time frame using an automated spot detection algorithm that considered spot intensity, shape, and hysteresis (see Figure S2). The center of each spot was found to subpixel resolution, then associated with the closest nucleus. Cases where multiple spots were associated with the same nucleus in the same frame were rare (< 10 instances per data set). These were resolved by inspection: the spot closest to the location of spots associated with that same nucleus in adjacent time frames was chosen. A nucleus was considered actively transcribing at a given time frame if a spot of transcription was associated with it.

QUANTIFICATION AND STATISTICAL ANALYSIS

Determining model parameters

All modeling was restricted to nuclei located in the center of the stripe 2 domain. To determine those nuclei, the time-dependent mean position of each nuclei was computed in units of percent of anterior-posterior axis length (AP). This mean position was computed over the time interval starting with the appearance of the first active transcription spot and ending with the disappearance of the last active spot within a single embryo. Every nucleus with a mean position within 2% AP of the mid-point of the stripe was considered within the center of the stripe and was included in the modeling analysis (Figure S3).

To derive the model parameters of Equation 2, we used maximum likelihood methods to directly fit the underlying active transcription observations as described in Friedman and Gelles. First, we made survival histograms of active transcription frequency binned by their dwell times (Figures 3B and 3C). The total frequency is given by the vertical axis intercept of this curve. This is equal to the inverse of the idle periods of Figures 3E and 3F and Table 3. The rate at which these curves fall off for increasing dwell time (i.e. the slope) is essentially the off rate of the active transcription dwell times; the initial slope is proportional to the inverse of the short characteristic time, τ_1 , and the slope at longer dwell times is proportional to the inverse of the long characteristic time, τ_2 . To determine the model parameters of Equation 2, the likelihood function was maximized using a modified version of that described in Ensign and Pande. The likelihood function was:

$$G_2^i(t|\tau_1^i,\tau_2^i,A^i) = \prod_i^{L^i} P_{\text{active transcription}}^i(t|\tau_1^i,\tau_2^i,A^i)$$
 (Equation 4)

with fit values τ_1 , τ_2 , and A. L^i is the total number of observed active transcription intervals for each condition i (eve2:wt, eve2:neutral, eve2[ZId]:neutral, eve2[Bcd]:neutral, or eve2[Dst]:neutral). The probability of each observation t for a given set of parameters, τ_1 , τ_2 , and t is given by Equation 2. The product of the probability of all observations (Equation 4) was maximized numerically by systematically varying the parameter values using the Nelder-Mead algorithm; the maximization was robust against a range of initial guesses spanning an order of magnitude. In practice, this meant using the sum of the natural logarithm of Equation 2 (the sum of the log of Equation 2 is equivalent to the log of Equation 4) in part because the product of the probabilities yielded exceedingly small numbers. Thus the likelihood that the computed distribution represents the distribution of observations is maximized. We did not directly fit the cumulative frequency distribution using conventional fitting procedures that assume independent errors because each point in the curve includes the random errors of all points to the left. The data from two imaging replicates for each transgenic reporter were combined and treated as a single dataset, as is typical for analysis of fluorescence spectroscopy experiments (e.g., Harden et al. 16).

The mean idle period values (Equation 3) were computed for each transgenic reporter by summing the total time that transcription was not detected within each active nucleus. This total inactive time included both the time between active transcription intervals as well as the time between the end of the final active interval and gastrulation (Figure S8, black regions). The total inactive time, L^i , was then divided by the number of inactive intervals, n^i . The choice for including the time between the final active interval and gastrulation is explained in Figure S9. In Figure S9 we also justify our use of mean idle period as a representative measure of the idle distributions. To do so, we invoked a bi-exponential model and fit the distributions in the same way that is described above for active transcription.

To determine the first passage model parameters (Equation 1), we again used the maximum likelihood methods described above. We chose to jointly fit the gamma scale parameter, τ_0 , to all conditions while simultaneously fitting the active fraction, A_f^i , and the gamma shape parameter, k^i , to each condition individually. Alternatively, we could have globally fit k while fitting A_f and τ_0 individually to each condition. We chose the former for a couple reasons. First, there is precedent: Dufourt et al. made this same choice. Second, this choice reflects a mechanism where the kinetic pathway is regulated when a TF increases the rate of a select number of rate limiting steps to make them relatively fast, rather than a TF modestly increasing the rate of all rate limiting steps in a pathway, although the latter is a formal possibility. This idea is fleshed out in Scholes et al.²

We maximized the likelihood function:

$$G_0^i(t|\tau_0, k^i, A_f^i) = \prod_i P_{\text{no first passage}}^i(T_{\text{Max}}, k^i, A_f^i)^m \prod_{j=1}^{N^i-m} P_{\text{first passage}}^i(t|\tau_0, k^i, A_f^i)$$
(Equation 5)





 T_{Max} is the maximum observation time, i.e. the length of NC 14. N is the total number of nuclei within the center of the stripe. m is the number of nuclei located in the center of the stripe but in which a transcription spot never appears. $P_{first\ passage}^{i}$ is given in Equation 1. $P_{no\ first\ passage}^{i}$ is the probability a nucleus is active but does not display a transcription spot during NC 14. This accounts for the stochastic reality that, under a given set of kinetic parameters, it is possible that a nucleus does not display transcription because it does not have time to turn on before gastrulation. In this possibility, a nucleus is not being actively suppressed nor does it lack sufficient activating TF activity. Thus we consider it active, despite a lack of transcription signal. This term is necessary to accurately determine the active fraction of nuclei, A_f . We maximized the sum of the logarithms of $P^i_{first\ passage}$ and $P^i_{no\ first\ passage}$ instead of their product because of the imprecision introduced by discrete observation of real, continuous phenomena.

To make the early distribution of active transcription lifetimes (Figure 3C; Table 2), we selected the 20% of lifetimes that first appear in any nucleus for each imaging replicate (e.g. 61/307 lifetimes for one replicate of eve2:wt). The remaining active transcription observations made up the later distribution (Figure S7; Table 2). The same method was used to separate the idle period distributions into early (Figure 3F; Table 3) and later (Table 3) subset distributions.

Error analysis

All parameter errors were estimated by bootstrapping. 114 Briefly, for each measurement (e.g. active transcription lifetimes, idle periods, first passage time) we generate 10,000 simulated data sets for each construct. To generate these, we randomly sample with replacement from the experimental observations. Bootstrapping of the first passage time distribution is an illustrative example. The eve2:wt experimental data set contained 88 nuclei within the center of the stripe. From these 88 nuclei, 88 observations were made. Some of these observations were a first passage time (from nuclei that displayed at least one instance of active transcription) and some of these observations represented nuclei that never displayed transcription. Thus each simulated eve2:wt data set contained 88 observations drawn randomly with replacement from the experimental data. These simulated data sets were subsequently analyzed with the same methods that were applied to the experimental data sets, as described above. A distribution of values was thus generated for each kinetic parameter. Standard statistical methods were then used to find the standard deviation of each parameter. We report these as error values in all tables and the bar charts.

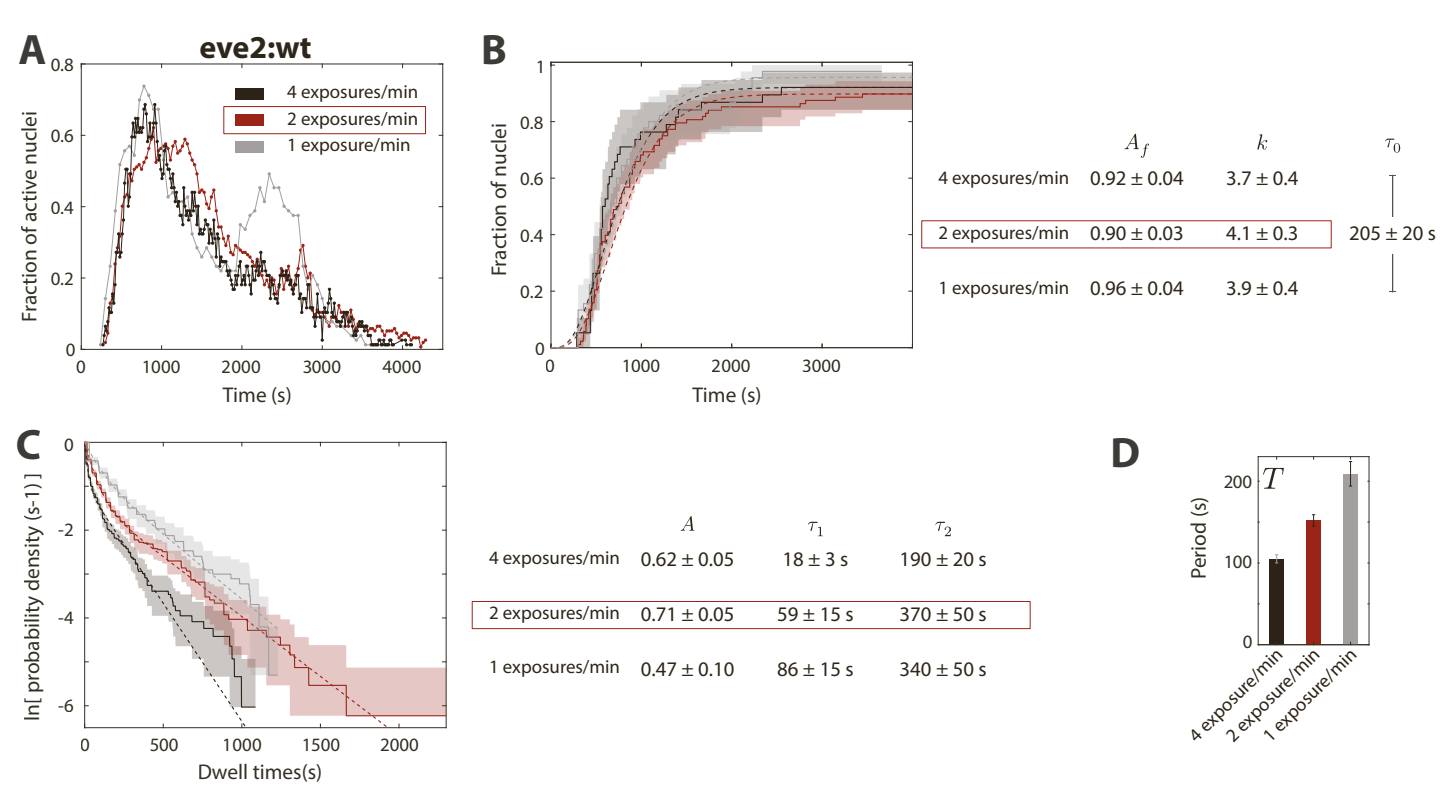
The shaded error regions of the frequency survival and cumulative first passage plots were also determined by bootstrapping. These regions represent the 90% confidence intervals, i.e. 90% of the simulated datasets fall within this range.

Cell Systems, Volume 14

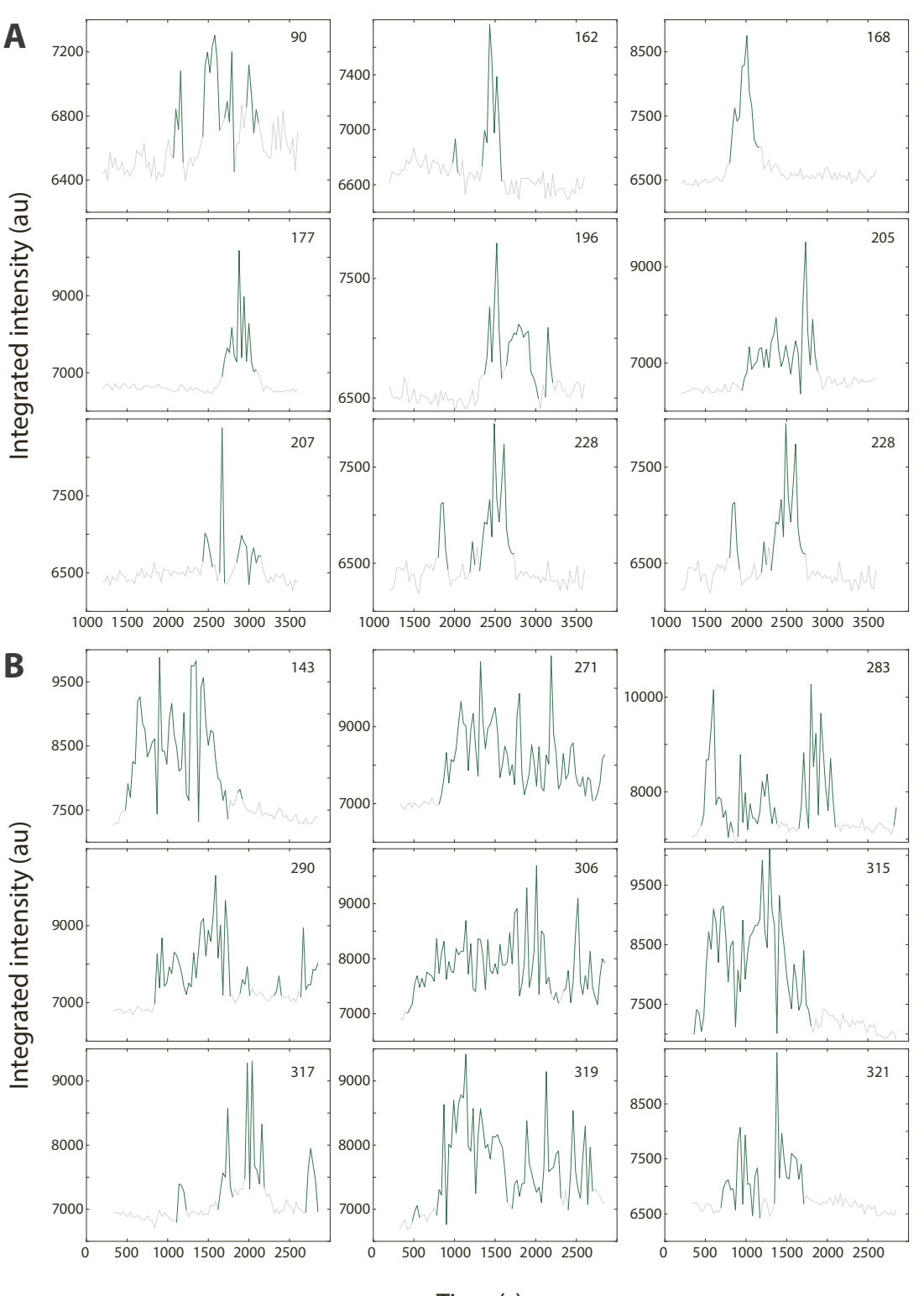
Supplemental information

Transcriptional activators in the early *Drosophila* embryo perform different kinetic roles

Timothy T. Harden, Ben J. Vincent, and Angela H. DePace

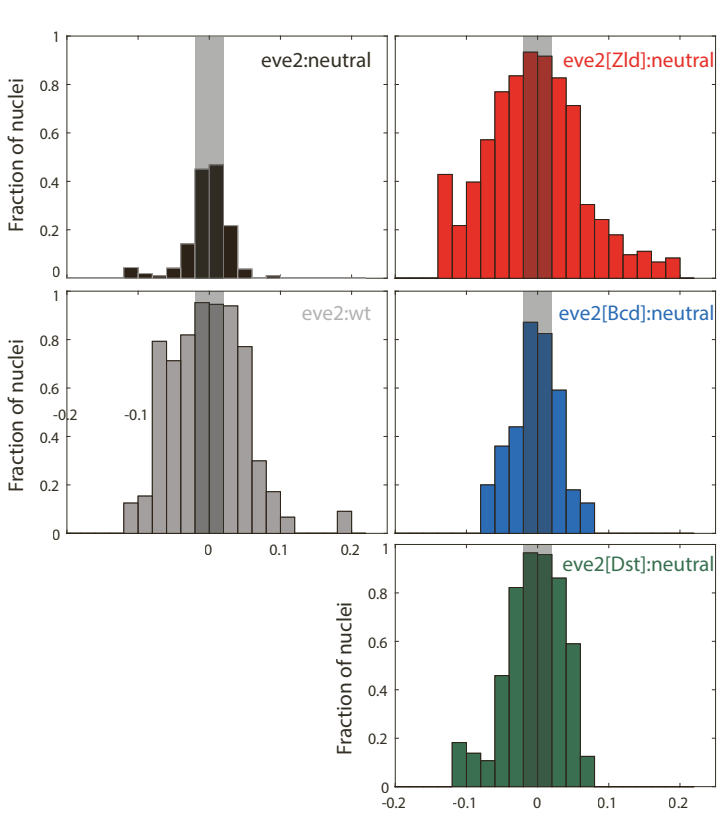


Supplemental Figure 1. Effects of laser exposure and image acquisition frequency on kinetic measurements. To assess if any distributions or kinetic parameters were meaningfully impacted by imaging conditions, including photobleaching, we repeated the eve2:wt experiment using two additional laser exposure frequencies: 4 exposures/minute and 1 exposure/minute. The data in all other figures, including for eve2:wt, was collected using 2 exposures/minute. (A) Dynamic transcription profiles during NC 14 as in Fig. 1D. The data for eve2:wt in Fig. 1D is reproduced here (dark red) alongside the 4 exposures/minute and 1 exposure/minute data. The three curves closely agree with one another throughout NC 14, with deviations attributable to experimental and biological noise. This suggests that the effects of laser exposure across the entire experiment, if any, are relatively small. (B) First passage into active transcription distributions with model fit (dashed lines), as in Fig. 2B; model parameters on the right. As would be expected for measurements drawn from early in the experiment (acquisition begins sometime during the previous nuclear cycle, which typically lasts for 10 - 13 minutes), both the distributions and the model parameters agree within experimental error. These measurements are not impacted by photobleaching. (C) Cumulative lifetime distributions and model parameters of active transcription lifetimes, as in Fig. 3B. The model parameters belie effects due to imaging conditions. The lower fraction of short lived events (parameter A) for 1 exp/min indicates that a subset of events are too short to be detected under this less frequent image acquisition. Conversely, both characteristic lifetimes (τ_1 and τ_2) are shorter for 4 exp/min, indicating that these measurements are likely artificially shortened by the increased laser exposure (i.e. photobleaching). (D) Barchart of mean idle periods, T, as in Fig. 3E. The value for the 1 exp/min acquisition was meaningfully impacted by acquisition frequency. As was seen for the active transcription intervals in (C), infrequent acquisition leads to short idle periods going undetected. Speeding up the frequency of acquisition to 4 exposures/minute, on the other hand, slightly increased the number of short idle periods that were detected, presumably due to photobleaching, although the two values are relatively close (105 \pm 5 s versus 152 \pm 7 s). Somewhat serendipitously, the imaging conditions for all data in this work are in a goldilocks zone: not too frequent so as to incur measurable photobleaching, but also not too infrequent so as to miss short interval events.



Time (s)

Supplemental Figure 2. Records of active transcription. Fluorescence emission records selected from either a single eve2:neutral experiment (A) or an eve2:wt experiment (B). Numbers in top right corners are arbitrarily assigned nucleus numbers. Green denotes the binary detection of active transcription; gray color marks intervals during which active transcription was not scored. The spot detection algorithm considered signal characteristics in addition to the integrated intensity shown in these records. At each frame, a band pass filter was applied to the MCP-GFP image to suppress noise and systematic variations across the field of view while keeping signal of a length scale commensurate with spots of transcription. Genuine transcription spots were detected by thresholding against both signal intensity and size (width); the same threshold values were used for each experiment. The center of the spots were then found to sub-pixel resolution, and a 2D gaussian was fit to the signal. To avoid artificially short active transcription intervals that arise from single frame signal dropout, hysteresis was included in the detection algorithm. At frame t, the spot intensity and width thresholds were lower if transcript signal was present at frame t-1 and t+1. This explains why in some records timepoints with low integrated intensity are scored as active transcription. For example, in record 143, there are noticeable dropouts at ~900 & 1400 s, including hysteresis ensures that this event is recorded as a single instance of transcription and not as three distinct events.



Position relative to stripe center (fraction of AP length)

Supplemental Figure 3. Kinetic analysis was restricted to nuclei located in the center of stripe 2.

Histograms of the fraction of active nuclei in a given spatial region of the embryo. Active is defined as having at least one instance of active transcription over the course of NC 14. Nuclei were binned according to their mean location over NC 14, shown on the horizontal axis in units of percent of the anterior-posterior axis length (see Methods). The center of the stripe is located at 0 on the horizontal axis. Gray shaded regions show the location of the nuclei analyzed in Figs. 2 and 3. There were 74 active nuclei and 166 nuclei total in the center of the stripe for eve2:neutral; 79/88 nuclei were active in the center of the strip for eve2:wt; 90/103 for eve2[ZId]:neutral; 67/91 for eve2[Bcd]:neutral; 86/93 for eve2[Dst]:neutral. Repressors, including Giant and Kruppel, act around either edge of the stripe to set the boundaries. Thus, analysis excluded these edge regions in an attempt to isolate activating TF activity from repressive TF activity.

SFig 4 B eve2:neutral eve2:neutral -1 0.8 -2 0.6 -3 0.4 -4 0.2 -5 0 0 eve2:wt -1 0.8 -2 0.6 -3 0.4 -4 0.2 -5 eve2:wt In[probability density (s⁻¹)] 0 1 Fraction of nuclei eve2[Zld]:neutral 0.8 -2 0.6 0.4 0.2 -5 eve2[Zld]:neutral 0 eve2[Bcd]:neutral 0.8 -2 0.6 -3 0.4 -4 0.2 -5 eve2[Bcd]:neutral 0 0 eve2[Dst]:neutral -1 0.8 -2 0.6 -3 0.4 -4 0.2 -5

eve2[Dst]:neutral

3000

0 500 1000

2000

Time (s)

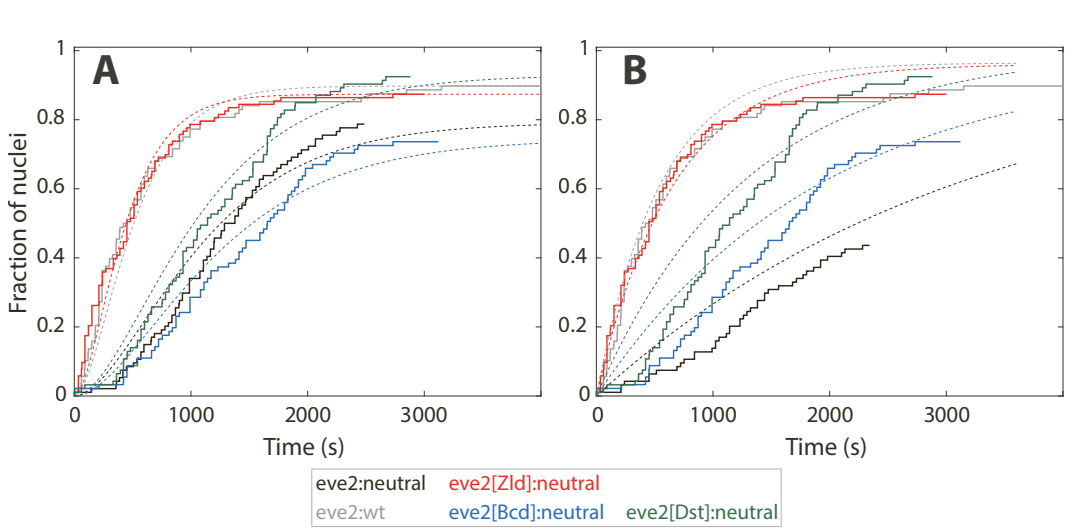
0 0 0

1000

1500 Dwell times(s)

2000

Supplemental Figure 4. Reproducibility of kinetic measurements between biological replicates. The first passage time (A) and active transcription lifetime (B) distributions for all biological replicates for each construct. As in Figs. 2B and 3B, respectively. Each shade represents a different replicate. The first passage time, active transcription, and idle period modeling all relied on the assumption that each nucleus is an independent measurement (see Methods). To justify this assumption we evaluated the embryo-to-embryo variability of these distributions statistically. To determine the probability that each replicate distribution came from the same parent distribution we used the Kolmogrov-Smirnov (K-S) test. For eve2:wt, eve2[Zld]:neutral, eve2[Bcd]:neutral, and eve2[Dst]:neutral, we ran a two sample K-S test between the two replicates. The tests all failed to reject the null hypothesis that each of the distributions were selected from the same parent distribution (p = 0.95). For those four constructs, the number of active nuclei in each replicate was adequate to provide sufficient statistics to draw conclusions using two replicates. For eve2:neutral, there were fewer active nuclei in the center of the stripe (19 ± 4 nuclei per replicate for eve2:neutral compared to 40 ± 5 for eve2:wt, 43 ± 1 for eve2[Zld]:neutral, 34 ± 1 for eve2[Bcd]:neutral, and 43 ± 2 for eve2[Dst]:neutral). Because there were fewer measurements for eve2:neutral, there were not sufficient statistics from two replicates. Therefore, we collected data from four replicates for eve2:neutral.



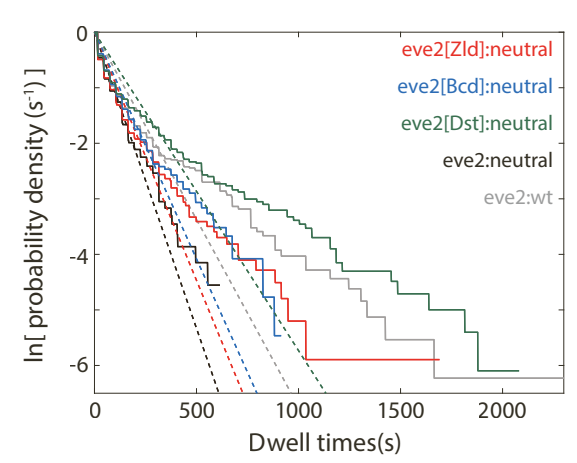
Supplemental Figure 5. Chemical kinetics models typically used to measure first passage rate constants cannot describe first passage into active transcription. (A) Cumulative first passage distributions (solid lines) as in Fig. 2B, but here the initial time delay between the end of anaphase and the first detection of transcription is ignored for each distribution. t = 0 is the time at which a transcription signal was first detected in the embryo, as has been done previously (Dufourt et al., 2018). The distributions are overlaid with a single step association model:

$$P_{\text{one step first passage}}^{i}\left(t\mid\tau^{i},A_{f}^{i}\right)=A_{f}^{i}\frac{1}{\tau^{i}}exp\left(-t/\tau^{i}\right)$$

with an active fraction and characteristic time fit parameter, τ and A_f^i , respectively (dotted lines). (B) The same data distributions as in (A), but overlaid with an association model of two *equal* rate limiting steps prior to first passage:

$$P_{\text{two step first passage}}^{i}\left(t\mid\tau^{i},A_{f}^{i}\right) = A_{f}^{i}\left(\frac{1}{\tau^{i}}\right)^{2}t\ exp\left(-t/\tau^{i}\right)$$

Even ignoring the initial time delay, neither of these models can reproduce the observed experimental distributions. In general, a lag in the initial association time, like that seen in Fig. 2B, requires a reaction path with multiple (more than two in this instance) rate limiting steps prior to activation, like that of Eq. 1.

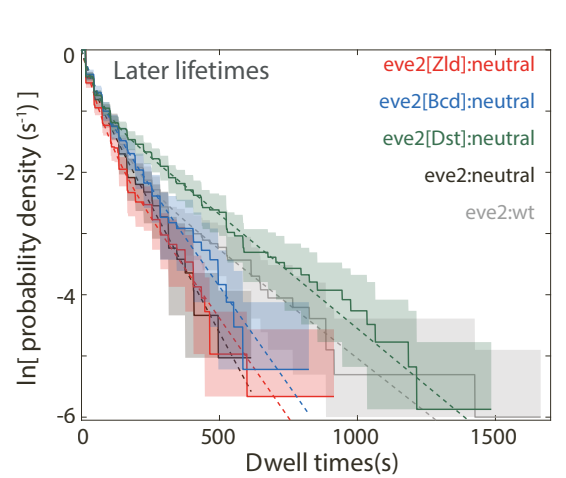


Supplemental Figure 6. A single characteristic lifetime is insufficient to model active transcription.

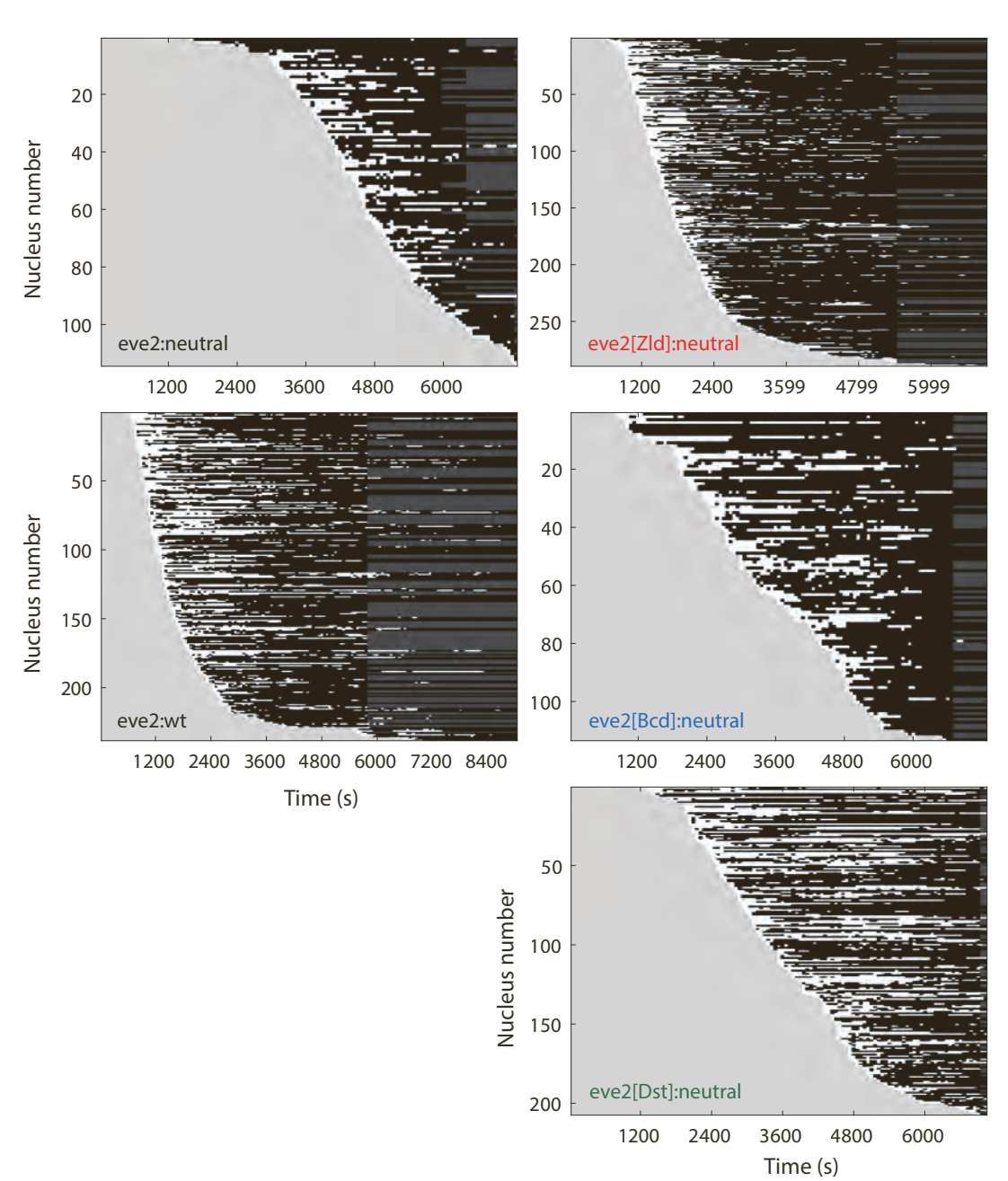
Cumulative lifetime distributions of active transcription lifetimes reproduced from Fig. 3B. For clarity, the shaded error regions have been omitted. In this instance, the data has been overlaid with a single exponential lifetime decay model:

$$P_{\text{active transcription}}^{i}\left(t\mid\tau^{i}\right) = \frac{1}{\tau^{i}}exp\left(-t/\tau^{i}\right)$$

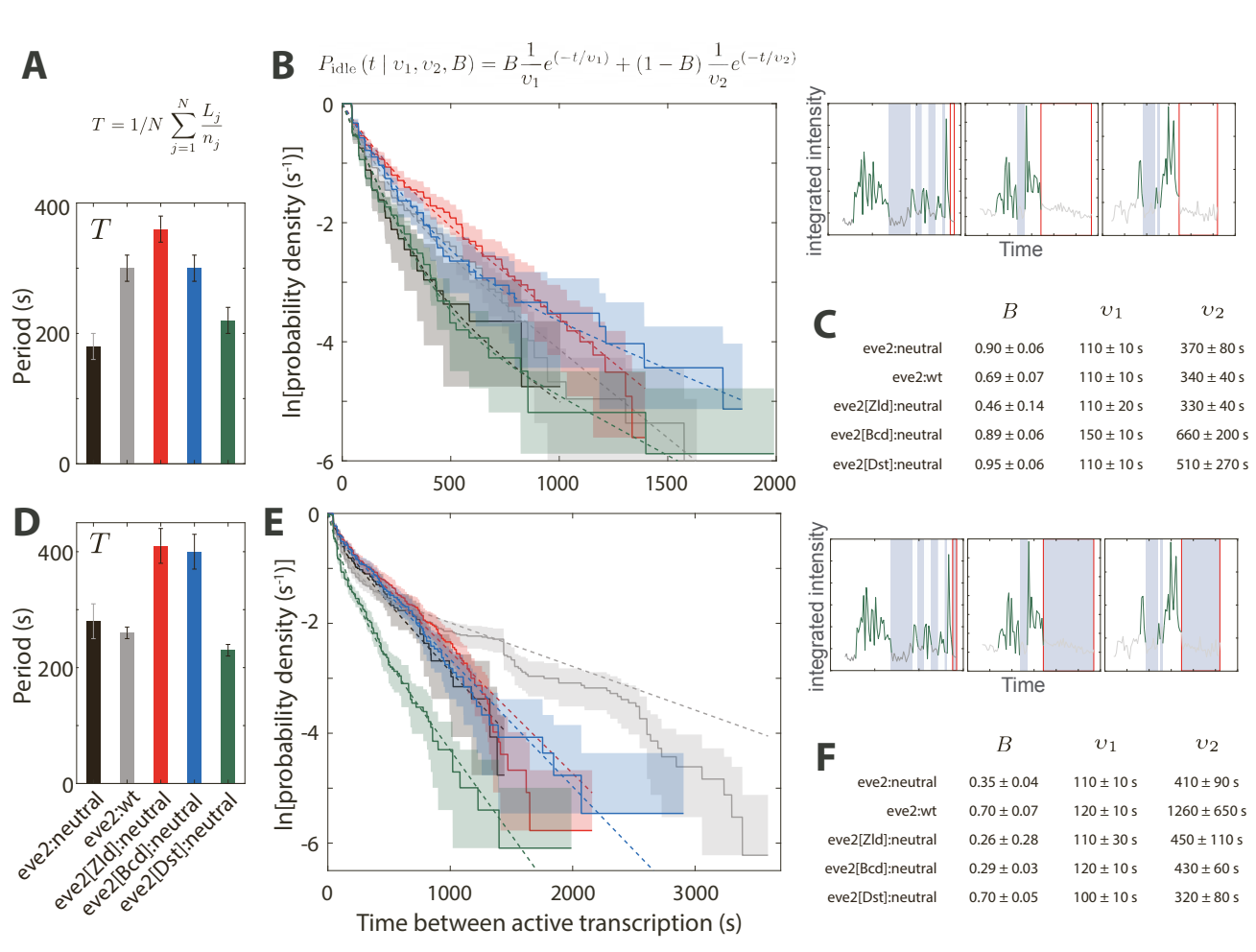
with a single fit parameter, τ^i (dotted lines). The distributions predicted by this model are not consistent with the experimental distributions.



Supplemental Figure 7. Active transcription kinetics later in NC 14. Cumulative lifetime distributions of active transcription, as in Fig. 3B, but omitting the 20% of lifetimes that are detected first in each nucleus. Put another way, the data shown here combined with the data of Fig. 3C make up the entire distribution shown in Fig. 3B. See Table 2 for parameter values. Shaded regions represent the 90% confidence intervals from bootstrapping methods.



Supplemental Figure 8. Binarized active transcription records for individual nuclei. Raster plots of binary MCP-GFP transcription signal in every nuclei with at least one instance of active transcription. These data are not limited to the center of the stripe, as opposed to all other data in this work which is drawn from the stripe center. Each row of these plots contains data from a single nucleus over the course of NC 14. Nuclei were sorted by time of first passage into active transcription. Colors indicate: first passage intervals (light gray), active transcription intervals (white), idle periods (black), and no data (dark gray) due to gastrulation of replicate embryos at different times. The cumulative length of time during which no transcription signal was detected, L^i , that was used to compute the mean idle period for each reporter was the sum of the black intervals that occur between white intervals (Eq. 3 and Fig. 3).



Supplemental Figure 9. Idle period distributions and models. (A-C) Mean idle period (A; reproduced from Fig. 3E), idle period distributions with bi-exponential model and example records depicting idle periods (B), and model parameter values (C). These data include times between active transcription intervals (blue highlights in the example records) but omit time between the last active transcription interval and the end of the experiment, which is about the time of gastrulation (red outlines in example records). (D-F) as in A-C, but include the times between the last active transcription interval and gastrulation (red outline intervals in records of E). Either set of data is valid as a measure of idle period. We chose that of A-C because, biologically, idle periods that occur between active transcription likely represent a different state than those that occur between active transcription and gastrulation. As such, we have chosen to report both distributions. Additionally, a bi-exponential model (B, top), its fit to the data (dashed curves), and the resultant parameters (C) explain why we chose to report the mean idle period as the measure of the distribution in the main text. The model parameters of C indicate that these distributions are closer to single exponential than bi-exponential. The fraction of short-lived events B is equal to one within error for most constructs. Therefore, we could not justify using a kinetic model that is more sophisticated than the mean of the distribution. Comparing the distributions of the five constructs in B and their mean values in A, the means give an accurate comparison of the distributions themselves. For example, the shortest mean idle periods, that of eve2[Dst]:neutral and eve2:neutral, are also the "shortest" distributions in B.